

Operator Spreading and the Emergence of Dissipative Hydrodynamics under Unitary Evolution with Conservation Laws

Vedika Khemani,¹ Ashvin Vishwanath,¹ and David A. Huse²

¹*Department of Physics, Harvard University, Cambridge, Massachusetts 02138, USA*

²*Department of Physics, Princeton University, Princeton, New Jersey 08544, USA*



(Received 12 December 2017; published 7 September 2018)

We study the scrambling of local quantum information in chaotic many-body systems in the presence of a locally conserved quantity like charge or energy that moves diffusively. The interplay between conservation laws and scrambling sheds light on the mechanism by which unitary quantum dynamics, which is reversible, gives rise to diffusive hydrodynamics, which is a slow dissipative process. We obtain our results in a random quantum circuit model that is constrained to have a conservation law. We find that a generic spreading operator consists of two parts: (i) a conserved part which comprises the weight of the spreading operator on the local conserved densities, whose dynamics is described by diffusive charge spreading; this conserved part also acts as a source that steadily emits a flux of (ii) nonconserved operators. This emission leads to dissipation in the operator hydrodynamics, with the dissipative process being the slow conversion of operator weight from local conserved operators to nonconserved, at a rate set by the local diffusion current. The emitted nonconserved parts then spread ballistically at a butterfly speed, thus becoming highly nonlocal and, hence, essentially nonobservable, thereby acting as the “reservoir” that facilitates the dissipation. In addition, we find that the nonconserved component develops a power-law tail behind its leading ballistic front due to the slow dynamics of the conserved components. This implies that the out-of-time-order commutator between two initially separated operators grows sharply upon the arrival of the ballistic front, but, in contrast to systems with no conservation laws, it develops a diffusive tail and approaches its asymptotic late-time value only as a power of time instead of exponentially. We also derive these results within an effective hydrodynamic description which contains multiple coupled diffusion equations.

DOI: [10.1103/PhysRevX.8.031057](https://doi.org/10.1103/PhysRevX.8.031057)

Subject Areas: Condensed Matter Physics,
Quantum Physics,
Quantum Information

I. INTRODUCTION

The nature of quantum dynamics and thermalization in isolated many-body systems is a topic of fundamental interest. Over the past few years, a remarkable confluence of theoretical progress and experimental advances in engineering and controlling isolated many-body quantum systems, especially in cold-atomic gases, has led us to reexamine our understanding of the very foundations of quantum statistical mechanics [1–3]. On the theory side, research in the field of many-body localization (MBL) [4–9] has revealed the existence of classes of generically interacting systems that do not obey quantum statistical mechanics, and understanding the nature of different MBL phases [10,11] and the transition(s) between MBL and thermalizing phases

[6,12–18] is an active area of research. Complementarily, the development of tools like the AdS/CFT duality [19,20] has led to new perspectives on the dynamics of thermalizing strongly interacting systems. This duality has been used to relate the physics of information scrambling in black holes to the process of thermalization in condensed-matter systems of interacting spins and/or particles [21–30].

One lens on the dynamics of isolated many-body quantum systems is provided by studying the spreading of initially local operators under the system’s unitary time evolution. In the Heisenberg picture, an initially local operator O_0 evolves into $O_0(t) = U^\dagger(t)O_0U(t)$ with support on a spatial region that grows with time. This spreading of $O_0(t)$ is reflected in the growth of the commutator between $O_0(t)$ and a typical local operator W_x with support near position x . If x is well away from the origin, then W_x initially commutes with O_0 . We define OTOC as the expectation value of the “out-of-time-order” commutator [31],

$$\mathcal{C}(x, t) = \frac{1}{2} \text{Tr} \rho^{\text{eq}} [O_0(t), W_x]^\dagger [O_0(t), W_x], \quad (1)$$

Published by the American Physical Society under the terms of the [Creative Commons Attribution 4.0 International license](https://creativecommons.org/licenses/by/4.0/). Further distribution of this work must maintain attribution to the author(s) and the published article’s title, journal citation, and DOI.

in an appropriate equilibrium Gibbs state ρ^{eq} . We will almost exclusively consider the infinite-temperature ensemble in which case the OTOC reduces to the squared Hilbert-Schmidt norm of the commutator. The OTOC is related to the commutator norm that appears in Lieb-Robinson bounds [32], and has received a great deal of attention recently as a diagnostic of information “scrambling” in quantum chaotic systems [21–30,33–35]. For a spin-1/2 chain of length L , a complete orthonormal basis for all operators is given by the 4^L “Pauli strings” \mathcal{S} , which are products of Pauli matrices on distinct sites. We can then express our spreading operator in this basis of Pauli strings:

$$O_0(t) = \sum_{\mathcal{S}} a_{\mathcal{S}}(t) \mathcal{S}. \quad (2)$$

The initially local operator O_0 consists only of strings \mathcal{S} that are the local identity at all sites except one or a few sites near the origin. But, with time, the strings that dominate this sum grow in spatial extent, containing nonidentity local operators at sites out to a “front” at a distance from the origin that grows with time. The OTOC remains near zero as long as the strings that dominate in $O_0(t)$ contain only local identities near position x , but it becomes nonzero once the operator front reaches this position.

In this paper, we are interested in understanding operator spreading and scrambling in the physically ubiquitous setting of thermalizing systems with one or a few local conservation laws that result in diffusive transport. This includes, for example, certain Hamiltonian models, since they do conserve energy, and in many cases energy transport is diffusive. It also includes certain Floquet systems which do not conserve energy but do conserve a charge or spin. We first investigate this question in a random tensor network spin chain model where the tensors are constrained to obey a single local $U(1)$ spin conservation law. We can derive a number of exact results in this setting, which we conjecture (and numerically verify) should also universally apply to Hamiltonian and Floquet spin chains with diffusive conserved quantities.

A set of recent papers has studied entanglement and operator dynamics in random tensor network models with no conservation laws [33,36–38]. A subset of these [37,38] showed that, despite the absence of traditional hydrodynamic conservation laws, unitarity alone amounts to a type of conservation law since the operator norm $\text{Tr}[O_0^\dagger(t)O_0(t)]$ is conserved, which means that the total weight of the operator on all Pauli strings $\sum_{\mathcal{S}} |a_{\mathcal{S}}|^2$ is conserved. This leads to an emergent “hydrodynamical” picture for describing operator spreading wherein, in one dimension, the dynamics of the operator front can be described by a distribution of biased random walkers (where the bias reflects the fact that it is more likely for an operator string to grow rather than to shrink) [37,38], while in higher dimensions the front is modeled by a random growth model

[36,37]. This leads to a picture in which the operator front propagates ballistically with “butterfly” speed v_B , while in low dimensions the width of the front grows as a sublinear power of time ($\sim\sqrt{t}$ in 1D) [37,38]. This means that the bulk of the total weight of $O_0(t)$ is contained in the spatial region lying within the “light cone” defined by the front whose spatial linear size grows linearly with time. Further, $O_0(t)$ is scrambled within the spatial region defined by the light cone and, with respect to some (but not all) measures, resembles an unconstrained random operator in this region [39].

In this work, we build on the picture above and study the interplay between the “actual” hydrodynamics governing the dissipative diffusion of conserved charges and the “emergent” hydrodynamics of unitary operator spreading in systems with conservation laws. Starting from a local operator that contains the conserved charge, we find that there is again a ballistically propagating front describing the operator spreading. However, unlike the fully non-conserved case, $O_0(t)$ has a significant (decreasing slowly as a power law in time) amount of weight on operator strings whose fronts lag far behind the main operator front. This can be understood as follows. Since conserved charges spread diffusively, the parts of $O_0(t)$ that overlap with the conserved charges are “left behind” in a region of linear size $\sim\sqrt{t}$ near the origin, even while the main operator front has reached distance $v_B t$. But the total weight of $O_0(t)$ on these local conserved operators decreases as a power law in time $\sim t^{-d/2}$ in d dimensions as the conserved density spreads diffusively. This loss of operator weight makes this diffusion effectively nonunitary and thus dissipative. But the full dynamics of the system is unitary, so the full operator weight is not lost. Instead, the dissipation due to the diffusive currents of the conserved density steadily converts operator weight from conserved to nonconserved operators, thus emitting a “flux” of nonconserved operators that then spread ballistically. This emitted flux is proportional to the square of the diffusive current, as expected for “Ohmic” dissipation. One point of view is that once the nonconserved operators start spreading ballistically, they rapidly become so highly nonlocal that they stop being observables. Then they can be viewed as effectively random, functioning as the bath whose entropy increases due to the dissipative diffusion.

An important point is that the conversion of operator weight from locally conserved to nonconserved (and non-local) happens at a power law *slow* rate set by the diffusion current, and thus the dissipation shows up as a slow *hydrodynamic* process in the operator dynamics. By contrast, in an unconstrained model, the dissipative conversion of operator weight from local to nonlocal happens on an $O(1)$ timescale and thus does not show up as a slow hydrodynamic process. An explicit elucidation of how unitary time evolution with conservation laws can lead to *slow* dissipative hydrodynamics is one of the main contributions of this work.

Moreover, in the models we study here, we can also study the unitary “inner workings” of this effective bath, following the spreading of the nonconserved parts of the operator. The bulk of these nonconserved operators are emitted almost immediately, near time $t = 0$, and these grow to form the leading operator front at distance $v_B t$ at time t . However, as a result of the conservation law, there is still significant weight left on the conserved parts even after the initial emission, and these continue to emit nonconserved operators at a slow rate that decreases only as a power law in time. Thus, those nonconserved parts of the operator that are emitted at a later time t_e have a front that lags behind the main operator front by distance $v_B t_e$. This leads to a power-law tail in the operator profile behind the front. By contrast, the unconstrained random circuit model does not show such a power-law tail, since in that case there are no slow dissipative modes, so no significant part of the operator has a front that lags substantially behind the main operator front. Figure 3 shows a sketch of the operator profile depicting all three regimes: (i) the diffusive conserved charges remaining near the origin, (ii) the ballistically moving front, and (iii) the power-law tail behind the front.

The picture that emerges from our study is of multiple coupled hydrodynamic equations. The first is the dissipative diffusion of the conserved quantity. This dissipation serves as the source of the ballistically spreading nonconserved operators. The dynamics of the fronts of these nonconserved operators is biased diffusion in 1D and a random growth model in higher dimensions [36,37]. Moreover, we find that the local operator content in the *interior* of the spreading operator is also governed by two coupled noisy diffusion equations, with the leading front of the operator serving as a moving boundary condition on these equations. And finally, there is at least one more “layer” of this hydrodynamics that governs the entanglement dynamics of the spreading operator [40].

The spatial profile of the spreading operator described above is also reflected in the behavior of the OTOC $\mathcal{C}(x, t)$ defined in Eq (1). We show that $\mathcal{C}(x, t)$ increases sharply when the ballistic operator front reaches x but, as a result of the power-law tails behind the main operator front, it only approaches its asymptotic late-time value as a power law in time. This is contrast to systems without conservation laws where there are no such power-law diffusive tails [37,38]. Our results help explain the numerical observations in Ref. [41], where this late-time power law in the OTOC was observed in systems with conservation laws.

We note that much recent work has focused on computing the OTOC at low temperatures in systems with energy conservation, and bounds on the growth of the OTOC have been derived in this setting [42]. On the other hand, random circuit models do not conserve energy, and thus, the “infinite-temperature” Gibbs ensemble is the only meaningful one for such models. Nevertheless, for circuit models

endowed with extra conservation laws like total spin or charge, the dynamics can be resolved into different spin sectors with the “chemical potential” μ now playing a role somewhat analogous to the inverse temperature β . We mostly focus on $\mu = 0$ in this work, while briefly addressing the $\mu \neq 0$ case.

We note that several papers have recently noted that quantum information can spread ballistically in systems with diffusively relaxing conserved charges [43–48]. This, by itself, is not that surprising since even MBL systems with no charge transport can show logarithmic spreading of entanglement [8,49]. Of these papers, Refs. [46–48] study a weakly interacting diffusive metal and, using a perturbative semiclassical scattering calculation, relate the butterfly speed v_B to the diffusion constant of the metal via a “Lyapunov exponent” which characterizes the exponential growth of “chaos” in this semiclassical setting as measured by the growth of the OTOC before the front arrives: $\mathcal{C}(x, t) \sim e^{-\lambda_L(x-v_B t)}$.

On the other hand, Refs. [43–45] numerically study fully quantum spin chains which cannot be treated semiclassically, and for which no prolonged period of exponential growth in the OTOC has been observed to date (the existence of a fully quantum Lyapunov exponent in spatially extended systems with small local Hilbert spaces and only short-range interactions, while perhaps expected, is a presently unresolved question [35,50,51]). In this fully quantum setting where semiclassical analytical methods do not apply, the aforementioned numerical papers [43–45] generally treat the diffusive charge relaxation and the ballistic information spreading as two independent numerical observations that do not interface with one another.

One of our main contributions in this work is to connect the diffusive charge dynamics with the ballistic front spreading in strongly quantum systems with local conservation laws into a composite picture for the operator profile, showing how the different regimes connect at different timescales and length scales. *En route*, we elucidate how reversible unitary dynamics can still display dissipative hydrodynamic modes, wherein the dissipative process is the conversion of operator weight from locally observable conserved parts to nonlocal and essentially unobservable nonconserved parts at a slow rate set by the local diffusion current of the conserved densities. Thus, while the von Neumann entropy of the full system is conserved under the unitary dynamics, we show how the local “observable” entropy can still increase at a slow hydrodynamic rate, very concretely illustrating a resolution of the fundamental tension between unitarity and dissipation in closed quantum systems.

The balance of this paper is structured as follows. We begin in Sec. II with a description of our constrained random unitary circuit model which has a local $U(1)$ conservation law total for total spin. This is followed by a detailed discussion of the spatial profile of spreading operators in Sec. III. We show that the conserved charges

evolve diffusively under the action of the circuit. The coupling between the charge conservation and unitarity produces a steady flux of operator weight from the diffusively spreading conserved components to ballistically spreading nonconserved components, leading to a power-law tail in the spatial profile of the operator weight. We present the coupled hydrodynamics describing this process. Next, in Sec. IV, we expose another layer of structure in the spreading operator by studying the local operator content of the highly nonlocal operator strings *within* the light cone defined by the leading ballistic front. We find that the distribution of different local operators is itself governed by a set of coupled noisy diffusion equations that “turn on” once the front passes a given position. In Sec. V, we turn to a discussion of OTOCs in this model, and find that the diffusive processes governing the shape and internal structure of the spreading operators lead to a late-time diffusive tail in OTOCs involving the conserved charges. We numerically verify that the universal aspects of our results also apply to more “physical” spin chains with energy and/or charge conservation in Sec. VI, and conclude in Sec. VII. Some additional details are discussed in Appendixes A–D.

II. RANDOM UNITARY CIRCUIT MODEL

As an explicit example where we can obtain analytical results, we consider a one-dimensional chain of length L sites where the degree of freedom on each site is the direct product of a spin $1/2$ (or qubit) and a qudit with Hilbert space dimension q . The time evolution is constrained to conserve the total z component of the spin $1/2$'s, which we call S_z^{tot} , while the qudits are not subject to any conservation laws. We note that we include the qudit at each site because some results can only be obtained analytically in the large- q limit, although some of our results do apply for all q , including the case $q = 1$ that has no qudits. For definiteness we take a finite L , but we will be interested in the behavior in the limit of infinite L .

Generalizing from Refs. [33,36–38], the time evolution is governed by a random quantum circuit comprising staggered layers of two-site unitary gates acting on even and odd spatial bonds at even and odd times, respectively (see Fig. 1). The time-evolution operator is given by $U(t) = \prod_{t'=1}^t U(t', t'-1)$, where

$$U(t', t'-1) = \begin{cases} \prod_i U_{2i, 2i+1} & \text{if } t' \text{ is even,} \\ \prod_i U_{2i-1, 2i} & \text{if } t' \text{ is odd.} \end{cases} \quad (3)$$

As a result of the conservation law, each two-site unitary gate $U_{i, i+1}$ is a $(4q^2 \times 4q^2)$ -dimensional block-diagonal matrix. Labeling the spin state on each site i as $(\uparrow a)_i$ or $(\downarrow b)_i$, where the first label is the spin state in the Pauli z basis and the second label is the qudit state, the structure of

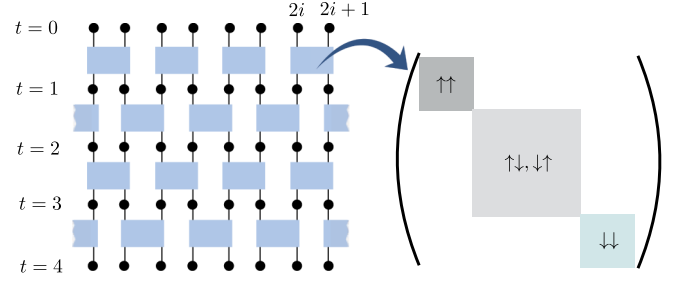


FIG. 1. Left: Diagram of the random unitary circuit. Each site (black dot) is the direct product of a two-state qubit and a q -state qudit. Each gate (blue box) locally conserves S_z^{tot} , the total z component of the two qubits it acts upon, and is thus a block-diagonal unitary of the form shown on the right, with each block of each gate independently Haar random. The smaller blocks do not flip the qubits and thus operate only on the two qudits, while the larger block also produces S_z^{tot} -conserving qubit “flip flops”.

$U_{i, i+1}$ looks like (i) a $(q^2 \times q^2)$ block acting in the $(\uparrow a)_i \otimes (\uparrow b)_{i+1}$ subspace, (ii) a $(2q^2 \times 2q^2)$ block acting in the $(\uparrow a)_i \otimes (\downarrow b)_{i+1}, (\downarrow a)_i \otimes (\uparrow b)_{i+1}$ subspace, and (iii) a $(q^2 \times q^2)$ block acting in the $(\downarrow a)_i \otimes (\downarrow b)_{i+1}$ subspace. Each of these blocks is a Haar-random unitary, and each block in each two-site gate is chosen independently of all others.

To characterize the time evolution of local operators, it is useful to define a complete orthonormal basis of operators on each site. For the spin, we can use the Pauli matrices on each site to define an on-site basis as

$$\{\sigma_i^{\mu=0,1,2,3}\} \equiv \{\mathbb{I}_i, r_i, l_i, z_i\} = \left\{ \mathbb{I}_i, \frac{\sigma_i^+}{\sqrt{2}}, \frac{\sigma_i^-}{\sqrt{2}}, \sigma_i^z \right\},$$

so r_i and l_i are suitably normalized spin-raising and -lowering operators, respectively. These basis operators all have a definite ΔS_z^{tot} (such as “raise or lower by one”) under the $U(1)$ symmetry that conserves S_z^{tot} and are thus more convenient than the Pauli $\sigma_i^{x/y}$ matrices for characterizing the $U(1)$ -conserving dynamics. For the qudit, one can construct higher-dimensional generalizations of the Pauli matrices $\{\sum_i^{\mu=0,1,\dots,q^2-1}\}$ that are normalized such that $\text{Tr}(\sum_i^{\mu\dagger} \sum_i^\nu)/q = \delta_{\mu\nu}$. Then, the tensor product $B_i^{\mu\nu} \equiv \sigma_i^\mu \otimes \sum_i^\nu$ generates a local basis for the $4q^2$ operators acting on each composite site i , denoted in shorthand as $(\mathbb{I}\Sigma^\nu)_i, (r\Sigma^\nu)_i, (l\Sigma^\nu)_i,$ and $(z\Sigma^\nu)_i$. Using this basis, the time-evolved operator $O(t)$ can be expanded as

$$O(t) = \sum_{\mathcal{S}} a_{\mathcal{S}}(t) \mathcal{S}, \quad (4)$$

where each generalized Pauli string \mathcal{S} is one of $(4q^2)^L$ basis product operators $\prod_i B_i^{\mu_i \nu_i}$. Since the basis strings satisfy $\text{Tr}[\mathcal{S}^\dagger \mathcal{S}]/(2q)^L = \delta_{\mathcal{S}\mathcal{S}'}$, the coefficients $a_{\mathcal{S}}$ can be obtained as $a_{\mathcal{S}}(t) = \text{Tr}[\mathcal{S}^\dagger O(t)]/(2q)^L$. Finally, we normalize the

initial operator O_0 such that $\text{Tr}[O_0^\dagger O_0] = (2q)^L$ which, by the unitarity of the dynamics, implies that the total weight of $O(t)$ on all strings \mathcal{S} is also normalized to 1:

$$\sum_{\mathcal{S}} |a_{\mathcal{S}}(t)|^2 = 1. \quad (5)$$

This sum rule is the effective conservation law due to unitarity [37,38].

There are a few classes of operators on site i that evolve differently under the action of this conserving unitary circuit. First, $(z\mathbb{I})_i$ measures the local conserved charge, and $(\mathbb{I})_i$ is the identity operator. The conservation law implies that S_z^{tot} is conserved so that

$$S_z^{\text{tot}} = \sum_i (z\mathbb{I})_i, \quad U(t)^\dagger S_z^{\text{tot}} U(t) = S_z^{\text{tot}}, \quad (6)$$

and the operators $(\mathbb{I})_i(\mathbb{I})_{i+1}$, $(z\mathbb{I})_i(z\mathbb{I})_{i+1}$, and $[(z\mathbb{I})_i(\mathbb{I})_{i+1} + (\mathbb{I})_i(z\mathbb{I})_{i+1}]/\sqrt{2}$ are left invariant by the action of all local gates $U_{i,i+1}$. Further, if one starts with an operator with a definite ΔS_z^{tot} under the $U(1)$ symmetry [for example, $(r\Sigma^\nu)_i$ raises the spin by one], the action of the circuit preserves this ΔS_z^{tot} . Appendix A summarizes the action of $U_{i,i+1}$ on all possible two-site operators.

It will be subsequently useful to separate the spreading operator into conserved and nonconserved pieces. To intuitively understand this separation, consider an initial density matrix

$$\rho(0) = (\mathbb{I}_{\text{all}} + A O_0)/(2q)^L, \quad (7)$$

where \mathbb{I}_{all} is the background equilibrium state which is the identity on the full system; $A O_0$ is a traceless local on-site perturbation at the origin to this equilibrium state, with O_0 normalized such that $\text{Tr}[O_0^\dagger O_0] = (2q)^L$; and A is the amplitude of this perturbation, which must be small enough so ρ remains non-negative. The system conserves S_z^{tot} Eq. (6) so that

$$\langle S_z^{\text{tot}} \rangle(t) = A \frac{\text{Tr}[O_0(t) S_z^{\text{tot}}]}{(2q)^L} = \langle S_z^{\text{tot}} \rangle(0) = A \frac{\text{Tr}[O_0 S_z^{\text{tot}}]}{(2q)^L}, \quad (8)$$

where $\langle \rangle(t)$ denotes expectation values in the state $\rho(t)$. If the perturbation injects some local charge at the origin, then, on general grounds, we expect this ‘‘extra’’ charge to spread diffusively so that $\langle (z\mathbb{I})_x \rangle \sim (1/\sqrt{t}) e^{-x^2/4Dt}$. We will see how this diffusion arises in operator language and explore its consequences for operator dynamics in this system.

To separate the part of $O_0(t)$ that has overlap with the conserved charges, we define $a_i^c(t)$ as the amplitude of the conserved charge $(z\mathbb{I})_i$ in the operator expansion of $O_0(t)$:

$$a_i^c(t) \equiv \frac{1}{(2q)^L} \text{Tr}[O_0(t)(z\mathbb{I})_i] = \langle (z\mathbb{I})_i \rangle(t). \quad (9)$$

The conserved charges, which act as $(z\mathbb{I})_i$ on site i and as the identity everywhere else, are a subset of the full basis of operator strings, and the ‘‘conserved part’’ of $O_0(t)$ is defined as the part of $O_0(t)$ with weight on these basis strings:

$$O_0^c(t) = \sum_i a_i^c(t) (z\mathbb{I})_i, \quad (10)$$

with the ‘‘nonconserved part’’ being the rest, $O_0^{\text{nc}}(t) = O_0(t) - O_0^c(t)$. Finally, the conservation law Eq. (8) requires

$$\sum_i a_i^c(t) = \text{const.} \quad (11)$$

The dynamics of operator spreading in this model is governed by the interplay between (i) this explicit charge conservation Eq. (11), which is a sum rule on the *amplitudes* of the conserved operators, and (ii) the conservation of the operator weight (which follows from unitarity), which is a sum rule on the *squares* of the amplitudes of *all* basis strings Eq. (5).

III. ‘‘SHAPE’’ OF SPREADING OPERATORS

A complete characterization of the spreading and scrambling of an initially local operator O_0 requires knowledge of the exponentially many coefficients $a_{\mathcal{S}}(t)$ in the expansion of $O_0(t)$ as in Eq. (4). Instead of doing this, we first consider a more coarse-grained approach and define the ‘‘right weight’’ $\rho_R(i, t)$ as the total weight in $O(t)$ of basis strings that end at site i , which means that they act as the identity on all sites to the right of site i , but act as a nonidentity on site i . This is the weight on all strings of the form $\mathcal{S} \sim (\prod_{k < i} B_k^{\mu_k \nu_k})(n)_i (\mathbb{I})_{i+1} (\mathbb{I})_{i+2} \dots (\mathbb{I})_L$, where $(n)_i \in \{(r\Sigma^\mu)_i, (l\Sigma^\mu)_i, (z\Sigma^\mu)_i, (\mathbb{I}\Sigma^{\mu > 0})_i\}$ denotes a nonidentity operator on site i :

$$\rho_R(i, t) = \sum_{\substack{\text{strings } \mathcal{S} \text{ with} \\ \text{rightmost non-} \\ \text{identity on site } i}} |a_{\mathcal{S}}|^2, \quad \sum_i \rho_R(i, t) = 1. \quad (12)$$

The conservation law on $\rho_R(i, t)$ which follows from unitarity Eq. (5) gives $\rho_R(i, t)$ the interpretation of an emergent local conserved ‘‘density,’’ and Refs. [37,38] showed that the (hydro)dynamics for $\rho_R(i, t)$ is governed by a biased diffusion equation. Of course, one can analogously define the left weight $\rho_L(i, t)$ and, together, these can be used to characterize some illuminating aspects of the spatial structure of the spreading operator (we consider other measures probing the local operator content inside the spreading operator in the next section).

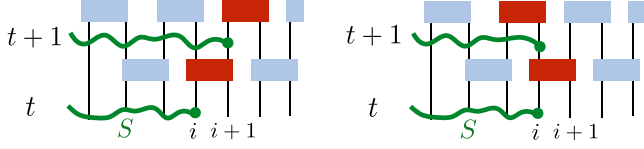


FIG. 2. A Pauli string S (green) with its rightmost nonidentity operator on site i at time t has its right front on the gate $(i, i + 1)$ (red). Under the action of the circuit, the front moves forward if the end point of the string moves to $(i + 1)$ at time $t + 1$ (left), while the front moves backward if the action of the circuit leaves the end point at site i (right).

It is instructive to first understand the dynamics of $\rho_R(i, t)$ in an unconstrained random circuit model in 1D with local Hilbert space dimension q . It was shown in Refs. [37,38] that the weighted distribution of the end points of the basis strings in the operator time evolve as biased random walkers, where the bias reflects the fact that it is more likely for the strings to grow rather than to shrink. If we define the “right front” of a string as the location of the rightmost unitary gate that sees a nonidentity, one can obtain the probabilities for the front to move forward or backward by noting that under the action of the front gate, all the $(q^4 - 1)$ nonidentity operators at the gate are produced with equal weights, on average. If the front gate is $U_{i,i+1}$, only $q^2 - 1$ of the operators that can be produced by this gate act as the identity on the right site of the gate $(i + 1)$, and each of these outcomes results in the front moving a step backward, an event with probability $p = [1/(q^2 + 1)]$. Because we define the front as living on gates (bonds) rather than sites, the even-odd structure of the circuit in time implies that the front moves backward when the end point of a string does not grow (illustrated in Fig. 2).

Then, from the theory of random walks, the mean location of the front after time t is $\langle x \rangle = (1 - 2p)t \equiv v_B t$, which defines the butterfly speed v_B , and the width of the front grows as $\sim \sqrt{D_\rho t}$, where $D_\rho = (1 - v_B^2)/2$ is the diffusivity of the resulting biased random walk. Evidently, the front location can be described by the emergent random walk hydrodynamics [37,38] $\partial_t \rho_R(x, t) = v_B \partial_x \rho_R(x, t) + D_\rho \partial_x^2 \rho_R(x, t)$, and the fact that the right-hand side of this equation is a total spatial derivative reflects the conservation of the emergent density ρ_R Eq. (12). Figure 3(c) shows a sketch of the Haar-averaged front for this random circuit evolution which, in the scaling limit $t, x \rightarrow \infty$ for $x \approx v_B t$, takes the form [37,38]

$$\rho_R^{\text{rand}}(x, t) = \frac{1}{\sqrt{4\pi D_\rho t}} e^{-(x - v_B t)^2 / 4D_\rho t}. \quad (13)$$

In the limit $q \rightarrow \infty$, the front becomes sharp and $v_B \sim 1 - (2/q^2) \rightarrow 1$, so that the front deterministically moves forward for all basis strings at each time step in this limit

[Fig. 3(d)]. Note that the geometry of the circuit limits the operator growth to at most one site on the left and right ends per time step. This imposes a strict upper bound on v_B set by the “causal limit speed” $v_{\text{CL}} = 1$, and v_B goes to this limit as $q \rightarrow \infty$.

Let us now turn to how this picture changes in the presence of an explicit $U(1)$ conservation law with diffusively spreading charges.

A. Spreading of the local conserved charge

Let us begin with the case when the initial operator is a conserved $U(1)$ charge located at the origin, $O_0 = (z\mathbb{I})_0$. In this case, the spatial structure of the operator shows three regimes: (i) a ballistic front, (ii) a power-law tail behind the front, and (iii) diffusively spreading charges near the origin.

1. Diffusion of conserved charge

We start by discussing the diffusive dynamics of the conserved parts of the operator. For the initial operator $O_0 = (z\mathbb{I})_0$, the initial conserved amplitudes are $a_i^c(0) = \delta_{i0}$ and the conservation laws Eqs. (8) and (11) give

$$\sum_i a_i^c(t) = 1. \quad (14)$$

When viewed as a perturbation to an equilibrium state Eq. (7), $O_0 = (z\mathbb{I})_0$ creates an excess of charge at the origin which should spread diffusively. Thus, on general grounds, at late times we expect $\langle (z\mathbb{I})_x \rangle(t) = a_x^c(t) \sim (1/\sqrt{t}) e^{-x^2/(4D_c t)}$, where D_c is the charge diffusivity. We now see how this arises.

To understand the evolution of $a_i^c(t)$, consider the action of a particular gate U_{12} on the superposition $[a_1^c(z\mathbb{I})_1 + a_2^c(z\mathbb{I})_2]$. It can be shown (Appendix C) that the action of a gate makes the average amplitudes \overline{a} equal on the two sites acted upon by it, while preserving the sum of amplitudes. That is, after the action of the gate, the Haar-averaged amplitudes are

$$\overline{a_1^c(t+1)} = \overline{a_2^c(t+1)} = \frac{\overline{a_1(t)} + \overline{a_2(t)}}{2}, \quad (15)$$

and the gate has produced a current between these two sites of the conserved charge that is $\sim [a_1(t) - a_2(t)] \sim \partial_x a(x, t)$. Note the “smoothing” action of the circuit, which locally makes the averaged amplitudes equal, and thus reduces $\partial_x a(x, t)$ in time. This action gives a binomial charge distribution (Appendix C):

$$\overline{a_i^c(t)} = \frac{1}{2^t} \binom{t-1}{\lfloor \frac{t-1}{2} \rfloor}, \quad (16)$$

which is an exact result true for all q including $q = 1$. If we coarse grain, in the scaling limit $x, t \rightarrow \infty$, we get

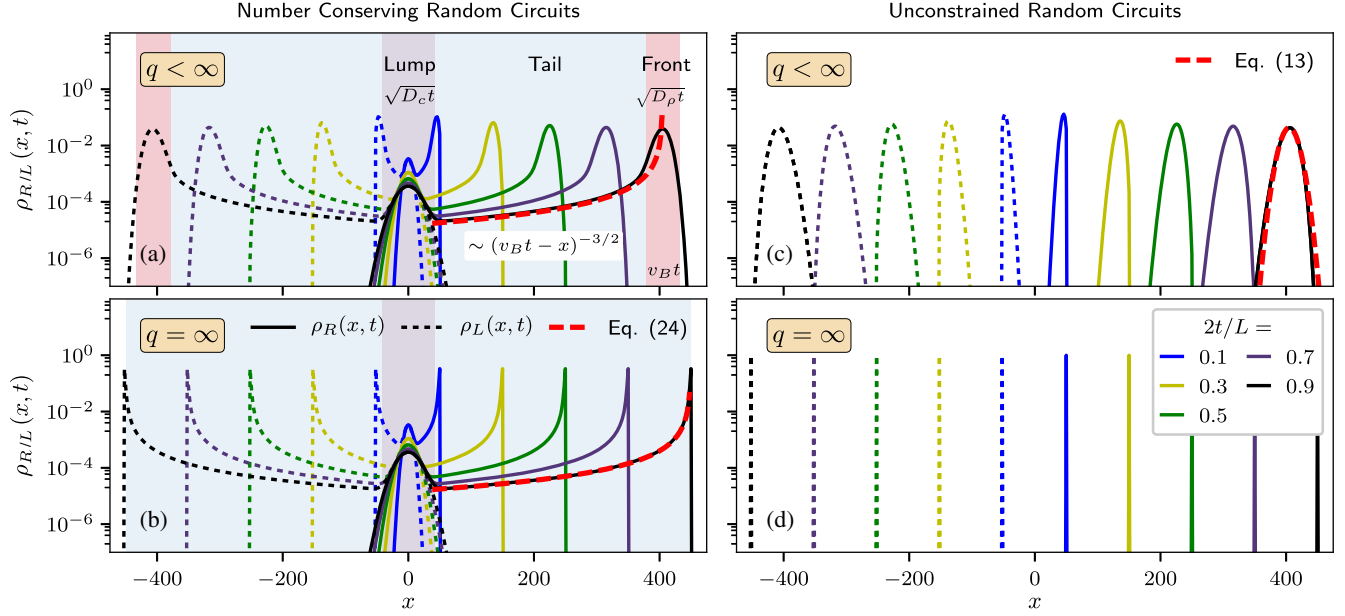


FIG. 3. (a),(b) Right/left-weight profiles $\rho_{R/L}(x, t)$ showing the spreading of an initially local conserved charge $(z\mathbb{I})_0(t)$ in a random circuit model with S_z^{tot} conservation in a system of size $L = 1000$ at different times t . These profiles depict three regimes. (i) A “lump” in the region $|x| \lesssim \sqrt{D_c t}$ reflecting the weight of the operator on diffusively spreading conserved charges (shaded purple). This lump emits ballistically spreading nonconserved operators at a slow power-law rate. This emission creates (ii) the leading ballistic “fronts” near $|x| \sim v_B t$ within which the majority of the operator right and left weight is contained (shaded red for the latest time). These leading fronts are from nonconserved operators emitted at early times and they are perfectly sharp at $q = \infty$, where $v_B = 1$ (b), and have a width $\sqrt{D_\rho t}$ for finite q (a). Finally, the slow emission also leads to (iii) diffusive tails $\sim (v_B t - |x|)^{-3/2}$ behind the leading fronts which reflect the operator weight in “lagging” fronts of nonconserved operator strings that were emitted at later times (shaded blue for the latest time). The curves in (a) are obtained via a simulation at $q = 3$, which takes into account the different processes (diffusion of charges, emission of nonconserved operators, and the biased diffusion of the nonconserved right and left weights) to order $1/q^2$. The red dashed curve is the exact infinite q answer for the “tail” Eq. (24). (c),(d) For comparison, $\rho_{R/L}(x, t)$ in an unconstrained random circuit model [37,38], where $z_0(t)$ is not “special.” Regimes (i) and (iii) do not exist in an unconstrained circuit, and the ballistically spreading operator fronts describe the entire right- and left-weight profiles. The fronts are again infinitely sharp at $q = \infty$ (d) and have a finite width $\sim \sqrt{D_\rho t}$ for $q < \infty$ (c).

$$\overline{a^c(x, t)} = \sqrt{\frac{1}{2\pi t}} e^{-x^2/2t}, \quad (17)$$

showing diffusion of the conserved charge with diffusion constant $D_c = 1/2$. If we consider similar random circuits acting on a system in higher dimensions $d > 1$, a similar diffusive behavior will be present, just with diffusion along all directions. It is noteworthy that as a consequence of the conservation law, the Haar-averaged amplitudes $\overline{a_i^c(t)}$ are nonzero [Eq. (16)]. In an unconstrained random circuit, only the squared weights $\overline{|a_S|^2}$ survive Haar averaging while all amplitudes average to zero. Likewise, in our model with S_z^{tot} conservation, certain off-diagonal products of amplitudes $\overline{a_S a_{S'}}^c$ can also survive Haar averaging (Appendix C), while all such averages are zero in the unconstrained model.

2. Ballistic front and power-law tails

We now turn to the effect of the diffusive dynamics on the shape of the spreading operator as measured by $\rho_R(i, t)$.

It is important to note that $\rho_R(i)$ measures the weights $|a_S|^2$ of all operator strings ending on i , while the preceding discussion was about the diffusive dynamics of the amplitudes a_i^c of only the conserved charges in the expansion of $O_0(t)$; these conserved operators are strings of length one site. Of course, the weight of $O_0(t)$ on a conserved charge at site i contributes to $\rho_R(i, t)$, and it is convenient to separate out this contribution:

$$\begin{aligned} \rho_R(i, t) &= |a_i^c(t)|^2 + \rho_R^{\text{nc}}(i, t) \\ &\equiv \rho^c(i, t) + \rho_R^{\text{nc}}(i, t), \end{aligned} \quad (18)$$

where ρ_R^{nc} denotes the right weight from all “nonconserved” operator strings that are not one of the conserved charges $(z\mathbb{I})_i$. Defining $\rho_{\text{tot}}^c \equiv \sum_i |a_i^c(t)|^2$ and $\rho_{\text{tot}}^{\text{nc}} \equiv \sum_i \rho_R^{\text{nc}}(i, t)$, we know from Eq. (12) that

$$\rho_{\text{tot}}^c + \rho_{\text{tot}}^{\text{nc}} = 1. \quad (19)$$

We will show that the total weight of $O_0(t)$ on the conserved charges ρ_{tot}^c decreases as a power law in time;

the conserved densities thus act as a source, continuously emitting a flux of nonconserved operators that spread ballistically and contribute to $\rho_{\text{tot}}^{\text{nc}}$ [52].

Let us see how this comes about. First, we show in Appendix C that the circuit-to-circuit variance in the conserved amplitudes is suppressed both in the large q and the late-time t limit:

$$\Delta_i^a(t) \equiv \overline{|a_i^c(t)|^2} - |\overline{a_i^c(t)}|^2 \sim \frac{1}{q^4} \frac{1}{t^2}, \quad (20)$$

while the leading term $|\overline{a_i^c(t)}|^2$ scales as $\sim 1/t$ Eq. (17). In this limit, $\Delta_i^a(t) \approx 0$ and $|\overline{a_i^c(t)}|^2 \approx \overline{|a_i^c(t)|^2}$. Then, the power law decrease in ρ_{tot}^c is obtained as

$$\overline{\rho_{\text{tot}}^c(t)} \approx \int dx |\overline{a_x^c(t)}|^2 = \int dx \frac{1}{2\pi t} e^{-x^2/t} = \frac{1}{2\sqrt{\pi t}}, \quad (21)$$

where we coarse grain at long times to obtain the penultimate equality, using Eq. (17). Likewise, in higher dimensions, this power law decrease will scale as $\rho_{\text{tot}}^c(t) \sim t^{-d/2}$, as can be easily seen by considering the higher dimensional generalization of Eq. (17). Because of the conservation of total density Eq. (19), this decrease in ρ_{tot}^c has to be compensated by a corresponding increase in $\rho_{\text{tot}}^{\text{nc}}$. Indeed, from the previous discussion, we see that the local decrease in ρ_{tot}^c (at $q = \infty$) due to action of a gate $U_{i,i+1}$ Eq. (15) is

$$-\delta\rho_i^c(t) = \frac{[a_i(t) - a_{i+1}(t)]^2}{2}. \quad (22)$$

This is the increase in $\rho_{\text{tot}}^{\text{nc}}$ that is locally generated at this gate, and this quantity is proportional to the square of the conserved quantity's local current. These newly produced nonconserved operators then evolve under the unitary dynamics and get converted to other nonconserved operators with increasing size. As in the case of the evolution of $\rho_R(x, t)$ for an unconstrained random circuit, the front of nonconserved operators (once generated) spreads ballistically, with $v_B = 1$ for $q = \infty$ since the likelihood of the front moving backward is again suppressed by $\sim 1/q^2$ (Appendix B). Further, in the $q = \infty$ limit, there is no “backflow” of density from nonconserved operators to conserved charges; this backflow only appears at order $1/q^4$. Thus, at $q = \infty$ and in the scaling limit, these considerations imply that

$$\rho_R^{\text{nc}}(x, t) = - \int_{x-v_B t}^x \frac{dy}{v_B} \frac{\partial \rho^c(y, t')}{\partial t'} \Big|_{(t'=t-(x-y)/v_B)}. \quad (23)$$

This expression tells a very natural story. The total nonconserved right weight at position x at time t is the integrated weight of all “fronts” emitted at locations y at times $t_y = t - (x - y)/v_B$ such that the front traveling with velocity v_B makes it to position x at time t . Moreover, since

the conserved charges are primarily spread within a distance $\sim \sqrt{D_c t}$ near the origin, the emission of nonconserved flux is only significant at locations within this diffusively spreading “lump of charge.” Then, at late time t , we see the three pieces in the shape of $\rho_R(x, t)$ mentioned earlier.

- (1) The diffusive “lump”: In the spatial region $|x| \lesssim \sqrt{D_c t}$ near the origin, the right weight comes almost entirely from the diffusively spreading conserved part of the operator, $\rho_R(x, t) \simeq |a^c(x, t)|^2$. As a result, the spreading operator has significant weight that is “left behind” near the starting position of the operator, and this weight decreases only as a power law in time $\sim t^{-d/2}$ in d dimensions Eq. (21). By contrast, a spreading operator in the unconstrained circuit model has negligible right weight (exponentially decreasing with t) near its initial location at late times.
- (2) The ballistic front: The leading ballistic operator front (at the right end) is at $x = v_B t$, and the weight at the leading front is from nonconserved operators that were emitted at early times. At $q = \infty$, the leading front is sharp, the right weight is strictly zero for $x > v_B t$ with $v_B = 1$, and the sharp front is due to those nonconserved operators that were emitted by gates acting at the precise edge of the causal light cone. At finite q , as in the unconstrained circuit model [37,38], the front distributions execute biased diffusion instead of strictly moving forward at each time step. This leads to an order $1/q^2$ correction in v_B : $v_B \simeq 1 - 8/(9q^2)$ (Appendix B) and gives the main operator front a nonzero width $\sim \sqrt{D_\rho t} \sim \sqrt{t/q^2}$. Thus, at finite q , the leading front is mostly due to nonconserved operators that were emitted at early times $t_e \lesssim \sqrt{D_\rho t}/v_B$. For systems in $d > 1$, the broadening of the front at finite q is given by a random growth model and grows (if at all) with a smaller power of time [36,37].
- (3) The diffusive tail: Finally, the fronts of nonconserved operator strings that were emitted at later times $t_e \gg \sqrt{D_\rho t}/v_B$ lag behind the leading front by $v_B t_e$, leading to the development of power-law tails in the right weight behind the main operator front. Consider positions x well separated from both the leading ballistic front and the diffusively spreading charge “lump” such that $\sqrt{D_c t} \ll x$ and $v_B t - x \gg \max\{D_\rho t, 1\}$. In this regime, at infinite q ,

$$\rho_R^{\text{nc}}(x, t) \approx \frac{1}{4\sqrt{\pi}(t - x/v_B)^{3/2}}, \quad (24)$$

which has a power-law tail in both space and time. Indeed, for x far separated from the lump, the diffusive charge lump emitting nonconserved flux

can be approximately treated as a point source with the same integrated weight, so that $\rho_R^{nc}(x, t)$ is given by the rate of change of the total conserved density in the lump $\partial\rho_{tot}^c/\partial t \sim t^{-3/2}$ at time $t_e = (t - x/v_B)$, which explains the 3/2 power Eq. (21). The leading functional dependence of this tail is the same at both infinite and finite q . For $d > 1$, the exponent in this power law is $1 + (d/2)$. By contrast, there is no such tail in the spatial profile of operators evolving under unconstrained circuits, since such circuits have no mechanism for generating fronts that significantly lag behind the main operator front. At $q = \infty$ for the unconstrained circuit, $\rho_R^{and} = \delta(x - v_B t)$, so there is strictly no tail; at finite q , the right weight behind the leading front for the unconstrained circuit falls off exponentially in time at locations x behind the front scaling with any fixed $0 \leq x/t < v_B$.

The left weight shows the same three regimes, by reflection symmetry.

Figure 3 shows $\rho_{R/L}(x, t)$ for both the unconstrained and charge-conserving random circuit models at infinite and finite q starting with an initially local conserved charge at the origin $(z\mathbb{I})_0$. The finite q plots are obtained via a simulation at $q = 3$ which takes into account the different processes (diffusion of charges, emission of nonconserved operators, and the biased diffusion of the nonconserved right and left weights) to order $1/q^2$. Higher-order corrections, including backflow from nonconserved densities to conserved charges, are not included. More explicitly, we use the exact q -independent expression for the amplitude of diffusing conserved charges Eq. (16) to obtain both ρ^c and the density of nonconserved operators generated on each bond at every time step Eq. (22). These newly generated nonconserved operators are then assumed to execute biased diffusion, just as in an unconstrained circuit, with a probability of moving backward equal to $4/(9q^2)$. The net density profile of nonconserved operators is obtained via a spatial and temporal convolution of the “source” terms on each bond at each time with the corresponding biased diffusion result for the evolution of $\rho_{R/L}$ in an unconstrained circuit Eq. (13) [with suitably modified expressions for v_B and D_ρ , correct to $O(1/q^2)$].

3. Hydrodynamic description

We now turn to a long-time hydrodynamic description of the coupled processes involving diffusion of the conserved “charge” and the propagation of the fronts of the non-conserved operators emitted from this diffusing conserved charge.

For specificity, we restrict our attention to systems that are statistically translationally invariant and inversion symmetric. In such systems the amplitudes of the conserved part of the operator obey an unbiased diffusion equation. In more than one dimension, the diffusivity may

not be isotropic; if that is the case, we rescale distances along the eigendirections of the diffusivity to make it isotropic:

$$\partial_t a^c(\mathbf{x}, t) = D_c \nabla^2 a^c(\mathbf{x}, t), \quad (25)$$

where $D_c = 1/2$ in our $d = 1$ random circuit model Eq. (17). This diffusion is also subject to noise, which will lead to fluctuations in a^c across different realizations of the random circuit but, as we discussed above Eq. (20), for initial operators that do contain the conserved quantity, the noise is a parametrically subleading correction to the amplitudes a^c in the late-time limit that is relevant to the hydrodynamics.

Diffusion is a dissipative process, and this is reflected here in the decrease with time of the total operator weight of the conserved part of the operator, $\rho_{tot}^c(t) = \int d\mathbf{x} |a^c(\mathbf{x}, t)|^2$. Since the full system is undergoing unitary dynamics, this loss of conserved operator weight means that weight is being converted to nonconserved operator weight. The density of local rate of this emission of nonconserved operators is $2D_c |\nabla a^c|^2$ Eq. (22), where we show that this coefficient is $2D_c$ below. Note that this dissipation is a slow hydrodynamic process—proportional to the conserved quantity’s local current squared, as in Ohm’s law. These “emitted” nonconserved operators then spread rapidly, becoming highly nonlocal. This is an example of a presumably much more general picture of how dissipative processes happen within closed systems undergoing unitary dynamics: Correlations captured by low-order observables are moved by the unitary dynamics to highly nonlocal, and thus effectively nonobservable operators. Dissipation in such closed systems is thus the “hiding” of correlations in highly nonlocal operators so that the correlations that remain detectable to low-order observables are reduced and thus the observable entropy increases, even though the von Neumann entropy of the full system remains unchanged.

To more explicitly define the observable entropy, consider the density matrix $\rho(t) = [1/(2q)^L][1 + O(t)]$. By unitarity, the von Neumann entropy of this state is independent of time. Now, if we consider the conserved part of this state $\rho^c(t) = [1/(2q)^L][1 + O^c(t)]$, then the entropy of this state is $S^c(t) = \text{Tr}[\rho^c(t) \log \rho^c(t)] = L \log(2q) - [1/(2q)^L] \text{Tr}[O^c(t)^2/2] + \dots$, considering only the leading term in an expansion in powers of $O^c(t)$, which is valid due to the smallness of O^c at late times. Thus, $S^c(t) = S_\infty^{eq} - \rho_{tot}^c(t)/2 + \dots$. So, $S^c(t)$ increases (towards the infinite-temperature equilibrium value) at a rate proportional to the power law slow rate of decrease of conserved weight $\rho_{tot}^c(t)$ Eq. (21). Since the conserved operators are local (single site), $\rho^c(t)$ is observable and $S^c(t)$ is a good proxy for the observable entropy. More generally, one should define the observable part of a state as comprising all local (say, single-site) operators rather than just the

conserved ones. However, the rate of increase of $S^{\text{obs}}(t)$ will still be dominated by the conserved parts since the weight on these only decreases as a power law in time, in contrast to the exponential in time decrease in the weight of local nonconserved operators. This is the reason why the increase in observable entropy in an unconstrained circuit, while present, is not a hydrodynamically slow process while models with conservation law show a power law slow increase in the observable entropy at a rate proportional to the local diffusion current Eq. (22).

Next, the dynamics of the spreading of the front of the emitted nonconserved operators is given by a random and nonlinear growth model for $d > 1$, which we do not discuss further here [36,37]. For $d = 1$, the weighted distributions of the fronts of the spreading strings move by biased diffusion [37,38]. We focus on the right-moving front, but the left-moving front is doing the same thing, just spatially reflected so it moves in the opposite direction.

Thus, the leading-order continuum hydrodynamics in $d = 1$ of the right density $\rho_R^{\text{nc}}(x, t)$ is described by a diffusion equation with drift and a source term representing the emission of nonconserved operators from local gradients in $a^c(x, t)$:

$$\partial_t \rho_R^{\text{nc}}(x, t) = v_B \partial_x \rho_R^{\text{nc}}(x, t) + D_\rho \partial_x^2 \rho_R^{\text{nc}}(x, t) + 2D_c |\partial_x a^c(x, t)|^2, \quad (26)$$

where we show in Appendix B that the drift and diffusion constants are $v_B \simeq 1 - [8/(9q^2)]$ and $D_\rho \simeq [8/(9q^2)]$ neglecting corrections of order $1/q^4$ and higher. Further, it was shown in Refs. [37,38] that the circuit-to-circuit fluctuations in $\rho_R(x, t)$ [and hence $\rho_R^{\text{nc}}(x, t)$] scale with a parametrically smaller power of t , so we can ignore the noise in ρ_R^{nc} in the leading-order hydrodynamics. Thus, the coupled diffusion equations (25) and (26) describe the leading-order hydrodynamics for those aspects of the shape of the operator that are described by $\rho_R(x, t)$.

It is instructive to also directly consider the hydrodynamics for the total right weight, $\rho_R(x, t) = \rho_R^{\text{nc}}(x, t) + [a^c(x, t)]^2$, an exercise that explicitly reveals the form of the source term for ρ_R^{nc} in Eq. (26). Consider

$$\begin{aligned} \partial_t \rho_R(x, t) &= \partial_t \rho_R^{\text{nc}}(x, t) + \partial_t [a^c(x, t)]^2 \\ &= v_B \partial_x \rho_R^{\text{nc}}(x, t) + D_\rho \partial_x^2 \rho_R^{\text{nc}}(x, t) + \mathcal{S}^{\text{nc}}(x, t) \\ &\quad + D_c \partial_x^2 [a^c(x, t)]^2 - 2D_c |\partial_x a^c(x, t)|^2, \end{aligned} \quad (27)$$

where we have left the functional form of the source term \mathcal{S}^{nc} for ρ_R^{nc} undetermined, and we have used Eq. (25) in evaluating the time derivative for the squared amplitudes of the conserved charges. Note, however, that since $\int dx \rho_R(x, t)$ is conserved, the continuity equation requires that $\partial_t \rho_R(x, t)$ is the total spatial gradient of a current $\mathcal{J}(x, t)$. Thus, the two terms in Eq. (27) that are not spatial

derivatives must cancel each other (up to a total derivative), giving

$$\mathcal{S}^{\text{nc}}(x, t) = 2D_c |\partial_x a^c(x, t)|^2, \quad (28)$$

which gives the hydrodynamics for ρ_R^{nc} Eq. (26). With this relation,

$$\begin{aligned} \partial_t \rho_R(x, t) &= v_B \partial_x \rho_R^{\text{nc}}(x, t) + D_\rho \partial_x^2 \rho_R^{\text{nc}}(x, t) \\ &\quad + D_c \partial_x^2 [a^c(x, t)]^2, \end{aligned} \quad (29)$$

which nicely shows that the nonconserved part of ρ_R exhibits diffusive dynamics with a drift, while the conserved part simply diffuses with no net drift.

B. Spreading of local nonconserved operators

We now briefly describe the spreading of initial operators O_0 that are orthogonal to S_z^{tot} such that $\text{Tr}(O_0 S_z^{\text{tot}}) = 0$. These operators come in two categories: those with $\Delta S_z^{\text{tot}} \neq 0$ (such as the raising and lowering operators r_0 and l_0 with $\Delta S_z^{\text{tot}} = \pm 1$, respectively) and those with $\Delta S_z^{\text{tot}} = 0$ (such as $r_1 l_2$). The first category of operators only have weight on basis strings with the same $\Delta S^z \neq 0$ for all times, and thus remain orthogonal to each conserved charge $(z\mathbb{I})_i$ so that $a_i^c(t) = 0 \forall i, t$. Thus, in this case, $\rho_R(x, t) = \rho_R^{\text{nc}}(x, t)$, and these operators do not have any left or right weight that is left behind near the initial location due to slow diffusive dynamics. This means that their right-weight profile does not have diffusive tails and looks essentially the same as ρ_R for an operator spreading under the action of an unconstrained random circuit Eq. (13), albeit with different drift and diffusion coefficients. This can also be seen from the hydrodynamic equation (26) since the source term will be zero for this case. However, we show in the next section that the local operator content *within* the spreading operator, i.e., internal to the light cone, still shows power-law correlations due to the conservation law.

Let us now turn to the second category of initial operators with $\Delta S_z^{\text{tot}} = 0$. These include ‘‘dipole’’ operators of the form $O_{01}^{\text{dip}} = \{[(z\mathbb{I})_0 - (z\mathbb{I})_1]/\sqrt{2}\}$, which still contain the local conserved charges but with amplitudes that sum to zero. In this case, one can show that the coarse-grained Haar-averaged conserved amplitudes $a^c(x, t)$ look like the spatial derivative of the amplitudes obtained for the case starting with a monopole source Eq. (17):

$$\overline{a_{\text{dip}}^c(x, t)} \sim \frac{x}{t^{3/2}} e^{-x^2/2t}, \quad \int dx \overline{a_{\text{dip}}^c(x, t)} = 0. \quad (30)$$

Indeed, this is also easily obtained from the hydrodynamic diffusion equation (25) with a dipole initial condition. Then, the total conserved *weight* again decreases as a power law in time, but with a faster decay as compared to the monopole case: $\rho_{\text{tot}}^c(t) \sim t^{-3/2}$ in 1D. The conserved

densities again act as a source of nonconserved operators leading to a power-law tail in $\rho_R(x, t)$, but with scaling $1/(x - v_B t)^{5/2}$ in 1D, as is seen by considering the rate of change of $\rho_{\text{tot}}^c(t)$. For $q < \infty$, charge-neutral operators like $r_1 l_2$ create a dipole with nonzero probability at early times which then spreads as just described, again giving such a power-law tail in the asymptotic operator shape.

This brings us to a technical aside about the large q limit which is relevant for the spreading of nonconserved operators. An initial operator $(r\mathbb{I})_1(\mathbb{I})_2$ becomes a superposition of order q^4 operators, each with $\Delta S^z = 0$, under the action of the first gate. Only operators that act as the identity on the qudit spins (and as z on the spin $1/2$) have a chance of making a charge dipole and thereby contributing to the conserved weight ρ_{tot}^c —but these are suppressed in probability by $1/q^4$. This illustrates one aspect of the dynamics that is suppressed by the infinite q limit, namely the likelihood for certain operators to make dipoles and thus to pick up power-law tails in $\rho_R(x, t)$. As a related point, if one starts directly with the dipole operator O_{01}^{dip} as before, then the $q = \infty$ limit is sensitive to whether the dipole is acted upon by a single gate U_{01} at the first time step, or whether it is acted upon by the two gates U_{-10} and U_{12} . The latter case proceeds exactly as described above since each initial gate sees a conserved $(z\mathbb{I})$, while in the former case the single gate immediately converts the dipole to order q^4 nonconserved operators leading to a $1/q^4$ suppression in the power-law tail. This strong sensitivity to microscopic initial details in the spreading of this class of operators is a peculiarity of the large q limit.

C. Spreading of multilocal conserved operators

We now briefly address the spreading of initial Pauli strings that are a product of N conserved charges,

$$O_{i_1 i_2 \dots i_N}(t=0) = (z\mathbb{I})_{i_1} (z\mathbb{I})_{i_2} \dots (z\mathbb{I})_{i_N},$$

with the sites ordered so that $i_1 < i_2 < \dots < i_N$. The operator dynamics of such strings is also directly constrained by the conservation law since the conservation of S_z^{tot} implies the conservation of $(S_z^{\text{tot}})^N = \sum_{j_1, j_2, \dots, j_N} (z\mathbb{I})_{j_1} \dots (z\mathbb{I})_{j_N}$, and thus “multilocalized” strings of charges act as the “conserved densities” of this higher-order conservation law. Then, as in Eq. (14), the sum of all amplitudes $a_{j_1 j_2 \dots j_N}^c$ of the strings of z that appear in the expansion of $(S_z^{\text{tot}})^N$ is conserved in time. Further, if $O(t=0)$ has N conserved charges, then only amplitudes $\overline{a_S}$ on basis strings with *exactly* N conserved charges survive Haar averaging, even though the expansion $(S_z^{\text{tot}})^N$ involves basis strings with less than N charges [in fact, the relevant conserved operator is the appropriate weighted sum of $(S_z^{\text{tot}})^N$, $(S_z^{\text{tot}})^{N-2}$, etc., such that it contains only these basis strings of exactly N charges].

We can now ask about the time evolution of amplitudes of the form $a_{j_1 j_2 \dots j_N}$ with $j_1 < j_2 < \dots < j_N$. Note that if

all the j 's lie on different gates at a given time t , then we have independent diffusion of charges on each of the gates and action of the circuit simply averages all the intergate correlations and makes them equal. Indeed, if one starts in an infinitely large system with the charges in the initial string well spaced such that the “diffusive cones” of the individual charges never intersect, then $a_{j_1 j_2 \dots j_N}(t) \simeq [1/(\sqrt{4\pi D_c t})]^N \prod_{k=1}^N e^{-(j_k - i_k)^2 / 4D_c t}$, and these amplitudes decay with time parametrically faster than those for a single conserved charge. On the other hand, if we start with a finite density of charges such that the independently diffusing charges encounter each other on a gate, then we have to account for the “hard-core” interaction between these charges which is encoded in the invariance of $(z\mathbb{I})_i (z\mathbb{I})_{i+1}$ under the action of a gate. As a result of this, the diffusing charges can never pass each other and the coarse-grained problem is that of “single-file diffusion” of N particles with a hard-core contact interaction. This problem has been solved in the literature [53], and predicts that

$$\overline{a_{j_1 j_2 \dots j_N}^c}(t) = \sum_{\sigma \in S_N} \prod_{k=1}^N \frac{1}{\sqrt{4\pi D_c t}} e^{-[\sigma(j_k) - i_k]^2 / 4D_c t}, \quad (31)$$

where the sum is over all $N!$ permutations σ for the particle labels at time t , the initial locations of the charges are $i_1 \dots i_N$, and we require $j_1 < j_2 < \dots < j_N$.

Finally, note that initial strings that are products of conserved operators on some sites and nonconserved operators on other sites do not have any overlap with any of the conserved charges or their higher moments. All Haar-averaged amplitudes for all basis strings will be zero in this case (although two-point correlations of the amplitudes can still survive averaging). Further, even if there is initially a diffusive “cone” of locally conserved charges in the vicinity of a conserved operator in the initial string, these quickly lose their coherence upon encountering the ballistic cones emanating from the initial locations of the nonconserved operators.

IV. INTERNAL STRUCTURE OF SPREADING OPERATORS

So far, we have discussed the shape of the spreading operator in terms of the right weight $\rho_R(x, t)$; we have used this to describe the ballistic light cone within which the operator has spread, and the power-law tails in the distributions of right and left weights within the light cone. We now turn to another layer of structure in the “shape” of the spreading operator that is relevant, for example, for the resulting OTOCs. This is the weighted local distributions of the different qubit operators (\mathbb{I}, r, l, z) within the strings \mathcal{S} that make up the operator. For an unconstrained random circuit, the distribution of these local operators is uniform between the four operator types after the leading operator

front has passed a given location, but the distribution is highly biased towards identities before the front reaches. On the other hand, different operators are inequivalent in the conserving random circuit, leading to imbalances in these local densities that persist after the front passes. Indeed, the evolution of these local densities and their correlations are constrained by two further conservation laws that encode the fact that the unitary circuit conserves the action of the initial operator under the $U(1)$ symmetry. These are the conservation of the total “spin” s if one starts in a state with definite S_z^{tot} and the conservation of the net “raising charge” $\mathcal{R} \equiv \Delta S_z^{\text{tot}}$ of an operator. Further, we will see that these conservation laws are coupled to each other through suitably defined two-point correlations of charge or spin within the operator.

A. Conservation of raising charge

The action of the conserving circuit preserves the net raising charge $\mathcal{R} \equiv \Delta S_z^{\text{tot}}$ of an initial operator that starts with a definite ΔS_z^{tot} action. Concretely, for a given basis string \mathcal{S} , the local $\mathcal{R}_i = +1$ if the qubit operator in \mathcal{S} at site i is a raising operator r , while a lowering operator l has $\mathcal{R}_i = -1$, and z and \mathbb{I} have $\mathcal{R}_i = 0$. Note that \mathcal{R}_i is sensitive to neither the qudit operator content nor the operator content on all other sites. The unitary circuit conserves $\mathcal{R}_{\text{tot}} = \sum_i \mathcal{R}_i$ for operators that start with a definite \mathcal{R}_{tot} , and the operator’s local raising charge \mathcal{R}_i moves diffusively. Nevertheless, the circuit still converts a given basis string into a superposition of many strings each with different local patterns of \mathcal{R}_i (but with the same \mathcal{R}_{tot}), and this choice of strings means that the diffusion of raising charge is subject to noise. For example, if a unitary gate U_{12} acts on a two-site operator with $\mathcal{R}_{\text{tot}} = +1$ such as $(r\mathbb{I})_1(z\mathbb{I})_2$, the action of the gate produces a superposition of $(4q^4)$ two-site strings of the form $\{(ra)_1(\mathbb{I}b)_2, (ra)_1(zb)_2, (\mathbb{I}a)_1(rb)_2, (za)_1(rb)_2\}$, where a and b are arbitrary operators on the qudit and, within this ensemble of strings, the raising charge r is equally likely to be on either of the two sites acted upon by the gate (Appendix A). Of course, there is also noise from circuit-to-circuit fluctuations. If we average over the weighted ensemble of all strings within an operator that is evolved by a particular circuit and across circuits, then

$$\begin{aligned} \langle \mathcal{R}_i(t) \rangle &= \overline{\sum_{\substack{\text{strings } \mathcal{S}: \\ \mathcal{S}_i=(ra)}} |a_{\mathcal{S}}(t)|^2} - \overline{\sum_{\substack{\text{strings } \mathcal{S}: \\ \mathcal{S}_i=(la)}} |a_{\mathcal{S}}(t)|^2} \\ &\equiv \overline{\rho_r(i, t)} - \overline{\rho_l(i, t)} \end{aligned} \quad (32)$$

where $\langle \rangle$ denotes the joint average, and the notation $\mathcal{S}_i = (ra)$ means that the basis string acts as r on the spin 1/2 on site i and acts arbitrarily on the qudit. The last equality defines $\rho_{r/l}(i, t)$ as the weight on all basis strings in the operator expansion of $O(t)$ that locally act as r/l on the spin 1/2 on site i [one can analogously define $\rho_{\mathbb{I}/z}(i, t)$]. As

discussed above, the action of a gate U_{12} makes $\langle \mathcal{R}_i \rangle$ equal on the two sites and produces a raising charge current $\sim \partial_x \mathcal{R}(x, t)$:

$$\langle \mathcal{R}_1(t+1) \rangle = \langle \mathcal{R}_2(t+1) \rangle = \frac{\langle \mathcal{R}_1(t) \rangle + \langle \mathcal{R}_2(t) \rangle}{2}, \quad (33)$$

which is identical to the structure we had previously obtained for the dynamics of $\overline{a_i^c(t)}$ [Eq. (15)]. Thus, any initially local spatial distribution of $\langle \mathcal{R}_i \rangle$, for example, if $O_0 = (r\mathbb{I})_0$, spreads diffusively with diffusion constant $D_r = D_c$.

B. Conservation of spin

Likewise, there is a noisy diffusion process governing the conservation of total spin s which measures the projections onto definite S_z^{tot} states. If we rotate the local spin-1/2 operator basis to the projection “up” $u = (\mathbb{I} + z)/\sqrt{2}$ and “down” $d = (\mathbb{I} - z)/\sqrt{2}$ operators, then these are charged under s as $s = \pm 1$, respectively, while r, l have $s = 0$. In this basis, the operators $(u\mathbb{I})_i(u\mathbb{I})_{i+1}$, $(d\mathbb{I})_i(d\mathbb{I})_{i+1}$, and $[(u\mathbb{I})_i(d\mathbb{I})_{i+1} + (d\mathbb{I})_i(u\mathbb{I})_{i+1}]/\sqrt{2}$ are special and left invariant by the action of all two-site gates $U_{i,i+1}$, while the others mix between themselves in a manner that locally conserves $s_{\text{tot}} = \sum_i s_i$ on each gate. Thus, as before, the circuit conserves total s_{tot} while generating noise, so that after averaging over circuits and strings,

$$\begin{aligned} \langle s_i(t) \rangle &= \overline{\sum_{\substack{\text{strings } \mathcal{S}: \\ \mathcal{S}_i=(ua)}} |a_{\mathcal{S}}(t)|^2} - \overline{\sum_{\substack{\text{strings } \mathcal{S}: \\ \mathcal{S}_i=(da)}} |a_{\mathcal{S}}(t)|^2} \\ &\equiv \overline{\rho_u(i, t)} - \overline{\rho_d(i, t)} \end{aligned} \quad (34)$$

The action of a gate makes the average spin equal on the two sites:

$$\langle s_1(t+1) \rangle = \langle s_2(t+1) \rangle = \frac{\langle s_1(t) \rangle + \langle s_2(t) \rangle}{2}. \quad (35)$$

This again means that an initial spin polarization spreads diffusively with $D_s = D_c$. Note that this equality between diffusivities and the one for raising charge above Eq. (33) are not completely trivial statements, since D_c is for the *amplitudes* of the conserved operators that are a nonidentity only at one site, while D_s/D_r are for the local operator *weights* (amplitudes squared) of u/d ’s and r/l ’s within *all* strings, both conserved and nonconserved.

C. Coupling between spin and raising charge

If the initially local operator contains a nonzero net value of either of these two “charges,” then that charge will only spread diffusively. Thus, if we look near the ballistically moving operator front at long times, none of this initial charge can be there yet. Moreover, the action of the circuit is symmetric with respect to interchanging $r \leftrightarrow l$ and $u \leftrightarrow d$ (Appendix A), so that no new imbalances of the average

charges is created due to the action of the circuit. Thus, both these average charges are zero far from the initial location at late times, so that $\rho_r(x, t) = \rho_l(x, t)$ and $\rho_u(x, t) = \rho_d(x, t)$ for $|x| \gg \sqrt{D_c t}$. However, for all ballistically spreading operators, there is a next layer of structure in the *two-point* correlations of these charge densities that evolves diffusively near the front and influences some of the OTOCs. This structure stems from the initial condition in which the local operators are the identity on all sites except those near the origin, and these identities contribute only to $\rho_{u/d}$ and not to $\rho_{l/r}$. That is, *before* the front comes through, the operator is locally the identity which is an equal-amplitude linear combination of all strings that contain only u 's and d 's. On the other hand, in the final “local equilibrium” state of the operator, all local strings are equally likely a long time after the front has passed through (up to corrections that decay as a power law in L). This equilibrium state is reached via a noisy diffusion process that turns on at each position when the front passes through that position. The two-point correlations before the front passes through are $\langle \mathcal{R}_i \mathcal{R}_j \rangle = 0$ and $\langle s_i s_j \rangle = \delta_{ij}$, and these serve as the initial conditions on the diffusion process. This diffusion relaxes the initial imbalances between the *relative* density of local operators charged under spin and raising charge, in particular, the imbalance in $[\rho_u(x, t) + \rho_d(x, t)] - [\rho_r(x, t) + \rho_l(x, t)]$. We now see how this comes about.

To start, we look at the dynamics of *intergate* correlations. Consider two different gates acting at the same time t on sites $i, i + 1$ and $j, j + 1$. These two gates simply set all intergate correlations of each type equal, just as they do for the average densities:

$$\langle s_i s_j \rangle(t + 1) = \frac{\langle s_i s_j + s_i s_{j+1} + s_{i+1} s_j + s_{i+1} s_{j+1} \rangle(t)}{4}, \quad (36)$$

and seven other similar equations for the other intergate correlations of s and \mathcal{R} of the form $\langle \mathcal{R}_i \mathcal{R}_{j+1} \rangle(t + 1)$, etc. For concreteness, $s_i s_j = +1$ for strings that locally look like $u_i u_j / d_i d_j$ on sites i, j , and $s_i s_j = -1$ for strings that look like $u_i d_j / d_i u_j$, and is zero otherwise (analogous expressions for $\mathcal{R}_i \mathcal{R}_j$), and the equation above can be derived by looking at the action of the circuit gates on the different types of operators (Appendix A). The zero intergate correlations before the front comes through are indeed invariant under this dynamics. The coarse-grained diffusion equation for this two-point correlation for $x \neq y$ is thus

$$\partial_t \langle s(x) s(y) \rangle(t) = D_c (\partial_x^2 + \partial_y^2) \langle s(x) s(y) \rangle(t), \quad (37)$$

with $\langle \mathcal{R}(x) \mathcal{R}(y) \rangle(t)$ obeying the same equation. This is for $d = 1$, but the generalization of this and the results below to higher d seems straightforward.

Thus far, we have two separate diffusion processes governing the diffusion of raising charge \mathcal{R} and spin s correlations. In fact, these two processes are coupled once we consider the action within one gate on dipoles. The dipoles of \mathcal{R} are net raising-neutral operators like $\{(ra)_i (lb)_{i+1}, (la)_i (rb)_{i+1}\}$, while the dipoles of spin s are operators of the form $\{(ua)_i (db)_{i+1}, (da)_i (ub)_{i+1}\}$. The coupling between spin and raising charge stems from the fact that, while the total density of all such dipoles within one gate is locally conserved, the different dipole species mix among each other under the action of the gate. And it is this process that allows an initial operator that contains no r 's or l 's to relax to the final equilibrium where all local strings are equally likely. The precise “boundary conditions” that couple the above diffusion equations *within* one gate, i.e., at $x = y$, are q dependent and involve other correlations that can initially be well out of equilibrium just after the front passes.

The coupling between the charges can be simplified by looking at particular linear combinations of the $\langle \mathcal{R}_i \mathcal{R}_j \rangle$ and $\langle s_i s_j \rangle$ correlations. If we consider $\langle \mathcal{R}_i \mathcal{R}_j + s_i s_j \rangle$, this has the initial condition $\langle \mathcal{R}_i \mathcal{R}_j + s_i s_j \rangle = \delta_{ij}$. This initial condition is identical to the equilibrium final state where all strings are equally likely. And if we consider the action both within one gate and between two different gates, it does not change this quantity, which is therefore time independent. Thus, although we do have two coupled diffusion equations, it reduces to just one diffusion equation for

$$G_{ij}(t) \equiv \langle s_i s_j - \mathcal{R}_i \mathcal{R}_j \rangle(t) \quad (38)$$

for this initial state, which also has $G_{ij}(0) = \delta_{ij}$ as its initial condition. The local effective diffusivity due to the processes within one gate is, in general, q dependent and different from that when i and j are in different gates, but at long time this affects a “region” of G_{ij} that is a fraction $\sim \sqrt{1/t}$ of the distance $(i - j)$ over which it has spread. Thus, the leading coarse-grained long-time behavior of G_{ij} is

$$G(x, y, t) \approx \frac{1}{2\sqrt{\pi t}} e^{-(x-y)^2/4t}, \quad (39)$$

where the time t here is measured from the time when the front passes, say, the point $(x + y)/2$. Note that the effective diffusivity here is $2D_c = 1$, since we have independent diffusion at the locations x and y . In fact, at $q = \infty$, the evolution of $G_{ij}(t)$ within one gate is identical in structure to the intragate evolution and we can solve for G_{ij} exactly in this limit (Appendix D), and the coarse-grained answer agrees with Eq. (39). Finally, note that this form for $G(x, y, t)$ when evaluated at $x = y$ shows how the initial imbalances in the populations of u, d versus r, l decay diffusively away from the location of the front:

$$\begin{aligned}\Delta_{\mathcal{R}_s}(x, t) &\equiv G(x, x, t) \\ &= [\rho_u(x, t) + \rho_d(x, t)] - [\rho_r(x, t) + \rho_l(x, t)].\end{aligned}\quad (40)$$

For $q = \infty$, where $v_B = 1$, these imbalances can be evaluated exactly and they take the form

$$\begin{aligned}\Delta_{\mathcal{R}_s}(x, t) &= \frac{1}{3} \sum_{n=\lfloor \frac{t-|x|}{2} \rfloor}^{2\lfloor \frac{t-|x|}{2} \rfloor} \left(\frac{1}{3}\right)^n \binom{n}{2n-2\lfloor \frac{t-|x|}{2} \rfloor} \\ &\quad \times \binom{2n-2\lfloor \frac{t-|x|}{2} \rfloor}{n-\lfloor \frac{t-|x|}{2} \rfloor}\end{aligned}\quad (41)$$

$$\approx \frac{1}{2\sqrt{\pi(t-|x|/v_B)}},\quad (42)$$

where we have taken the late-time coarse-grained limit in the last line to evaluate the sum via a saddle-point approximation (Appendix D), and restored units. At finite q , we expect the leading functional dependence to still be the same, just with a reduced v_B . This equation, coupled with the fact that $\rho_l \approx \rho_r$ and $\rho_u \approx \rho_d$ away from the diffusive lump, allows us to solve for the local densities of the different operators, and this is sketched in Fig. 4, showing how all local densities diffusively approach the equilibrium value of $1/4$ after the front passes through. This diffusive relaxation of the

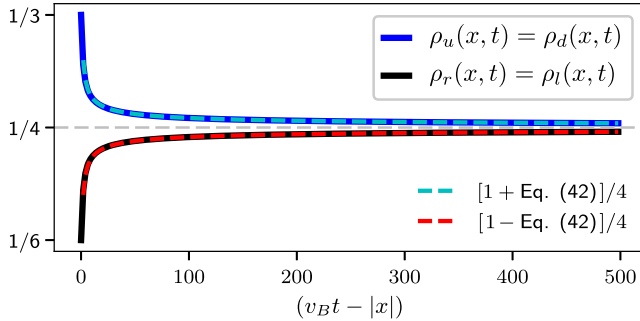


FIG. 4. Densities of local operators charged under “spin” and “raising action” behind the ballistic front of a spreading operator at $q = \infty$ and late times Eq. (41). $\rho_{u/d}(x, t)$ measures the local operator weight on site x on u/d operators that are charged under spin, while $\rho_{r/l}(x, t)$ measures the local weight on r/l operators that have raising charge. Outside the ballistic operator front (at $|x| > v_B t$), the spreading operator locally is purely identities which contribute equally to $\rho_{u/d} = 1/2$, but do not contribute to $\rho_{r/l} = 0$. The arrival of the front at a given site turns on a noisy coupled diffusion process between the spin and raising charges which relaxes the initially imbalanced densities of these charges to the final “equilibrium” value where all local operators are equally likely. Note that $\rho_u = \rho_d$ and $\rho_r = \rho_l$ in this regime since any initial imbalances in raising or spin charges spread only diffusively and are not present near the ballistic front at late times. Dashed lines plot the “coarse-grained” densities in the scaling limit Eq. (42).

imbalance leads to a power-law diffusive tail in certain OTOCs, as we see in the next section.

V. OUT-OF-TIME-ORDER COMMUTATORS

We now turn to measuring the out-of-time-order commutator between different classes of operators Eq. (1). We find that, in several cases, this quantity is sensitive to both the “shape” and the internal structure of spreading operators. If we consider the OTOC between two generic (initially) local operators, then this quantity is close to zero until the arrival of the ballistically spreading operator front and shows a sharp increase upon the arrival of the front. However, the OTOC for systems with local conservation laws also generically develops a “diffusive tail” and approaches its late-time asymptotic value only as a power law in time. Let us now see how this arises.

Define

$$C_{\alpha\beta}^{\mu}(x, t) = \frac{1}{2} \text{Tr}\{\rho_{\mu}^{\text{eq}} |[\sigma_0^{\alpha}(t), \sigma_x^{\beta}]|^2\},\quad (43)$$

where $\sigma_x^{\{\alpha=1,2,3\}} = \{r_x, l_x, z_x\}$ as before, we suppress the identity operators acting on the qudit spins on sites $0, x$ for notational simplicity, and

$$\rho_{\mu}^{\text{eq}} = \frac{e^{\mu S_z^{\text{tot}}}}{\text{Tr} e^{\mu S_z^{\text{tot}}}}\quad (44)$$

is the equilibrium “grand-canonical” ensemble at a particular chemical potential μ . Note that while the infinite-temperature average is the only equilibrium for a random circuit model with no energy conservation, for a circuit model with an extra conservation law (like ours), we may also consider a nonzero chemical potential which weights the different spin sectors as above. We focus on the equal-weight ensemble with $\mu = 0$ for the majority of this section, briefly commenting on $\mu \neq 0$ towards the end. We now study the OTOC for several different choices of α, β .

A. OTOC between $z_0(t)$ and r_x

Let us start with $\mu = 0, \alpha = 3 = z$, and $\beta = 1 = r$. Then,

$$C_{zr}^0(x, t) = \frac{1}{2} \text{Tr}\{\rho_0^{\text{eq}} |[z_0(t), r_x]|^2\},\quad (45)$$

and it is clear that only basis strings in the operator expansion of $z_0(t)$ that act as (la) or (za) on site x contribute to $C_{zr}^0(x, t)$. Then, using the commutation relations $[z_x, r_x] = 2r_x$ and $[l_x, r_x] = -2z_x$, and the orthonormality of basis strings, we get

$$C_{zr}^0(x, t) = \sum_{\substack{\text{strings } S: \\ S_x = \{la, za\}}} 2|a_S^z(t)|^2,$$

where the notation $a_S^z(t)$ denotes the amplitude of basis string S in the expansion of $z_0(t)$. A bit of algebra shows

$$\begin{aligned}
 \mathcal{C}_{zr}^0(x, t) = & 1 - \sum_{i < x} \rho_R(i, t) \\
 & + \sum_{\substack{\text{strings } \mathcal{S}: \\ \text{rhs}(\mathcal{S}) \geq x \text{ and} \\ \mathcal{S}_x = (l\alpha), (z\alpha)}} |a_{\mathcal{S}}^z|^2 - \sum_{\substack{\text{strings } \mathcal{S}: \\ \text{rhs}(\mathcal{S}) \geq x \text{ and} \\ \mathcal{S}_x = (l\alpha), (r\alpha)}} |a_{\mathcal{S}}^z|^2
 \end{aligned} \quad (46)$$

which is a useful way of writing this for $x > 0$; an analogous expression involving the left weight ρ_L can be written for $x < 0$.

Note that the first two terms in Eq. (46) are sensitive to the overall operator shape, namely, the right-weight profile of the spreading operator, while the latter two terms are sensitive to the local “internal” operator content after the front has passed site x . In random circuits with no conservation laws, all operator types are equally likely after the front has passed through and thus only the first two terms contribute substantially to the OTOC [37,38]. Notice that for this particular pair of operators, the second line measures the local raising charge \mathcal{R}_x Eq. (32) and the difference between the local densities of z 's and \mathbb{I} 's at site x after the front has passed x . As discussed in the previous section, there is no average raising charge away from the diffusing “lump” near the origin, and the difference in local densities of z 's versus \mathbb{I} 's is also zero *except* near the origin and right at the front. So, to leading order the second line in Eq. (46) vanishes in the region between the diffusive lump and the front. Further, since we start with zero raising charge, the only contribution to the second line comes from the imbalance between $\rho_z(x)$ and $\rho_{\mathbb{I}}(x)$. Indeed, all conserved operators $(z\mathbb{I})_i$ with $i \geq x$ contribute to $\rho_{\mathbb{I}}(x)$, while only $(z\mathbb{I})_x$ contributes to $\rho_z(x)$. These conserved operators are the leading source of the imbalance between $\rho_{\mathbb{I}}(x)$ and $\rho_z(x)$ near the origin. Nonconserved strings do not substantially contribute to the imbalance between $\rho_z(x)$ and $\rho_{\mathbb{I}}(x)$ away from the front. Then, putting it all together,

$$\begin{aligned}
 1 - \mathcal{C}_{zr}^0(x, t) \approx & \sum_{i < x} \rho_R^{\text{nc}}(i, t) + \sum_{i > x} \rho_L^{\text{nc}}(i, t) \\
 & + \rho_{\text{tot}}^c(t) - 2\rho^c(x, t),
 \end{aligned} \quad (47)$$

where we have separated the contributions from conserved and nonconserved operators Eq. (18) and used also the left weight ρ_L^{nc} to produce an expression that is valid at late time for all x . Since $\rho_{\text{tot}}^c(t) \sim t^{-1/2} \gg \rho^c(x, t) \sim t^{-1}$ at late times, the contribution of $\rho^c(x, t)$ is also subdominant at late times and is neglected below, although it is visible as a weak “dimple” in the diffusive regime near the origin in Fig. 5. Thus, away from the fronts and the diffusive regime near the origin, the OTOC for this pair of operators receives its primary contribution from the total right or left weights alone, just as in the unconstrained circuit [37,38]. We saw above that the right- and left-weight profiles for $z(t)$ show diffusive power-law tails, and these translate into diffusive tails for this OTOC as well.

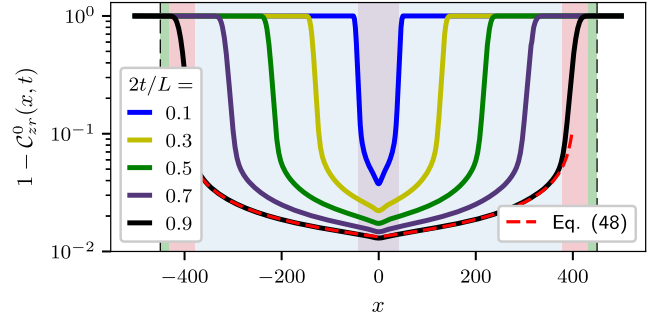


FIG. 5. One minus the out-of-time-order commutator (OTOC) between $z_0(t)$ and r_x at zero chemical potential \mathcal{C}_{zr}^0 plotted against x for a system of length $L = 1000$ at different times t showing the different regimes discussed in the text. For $|x| > t$ (outside the dashed vertical lines), the OTOC is strictly zero due to the locality of the circuit. In the region $v_B t < |x| < t$, which is inside the causal light cone but before the leading front arrives, the OTOC is exponentially small (green shaded area for the latest time). The arrival of the ballistic operator front ($|x| \sim v_B t$) leads to a strong increase in the OTOC from a value exponentially small to an $O(1)$ value (shaded red area for the latest time). However, diffusive tails in the operator shape or internal structure lead to diffusive power-law tails in space and time $\sim (x - v_B t)^{-1/2}$ in the late-time approach of the OTOC to its final value of 1 (shaded blue area for the latest time). By contrast, for an unconstrained random circuit (not shown), the OTOC at a given site approaches one exponentially quickly after the leading front passes [37,38]. The diffusive region near the origin $|x| \lesssim \sqrt{D_c t}$ (shaded purple) receives a subleading $1/t$ contribution from the conserved charges which shows up as a “dimple” in the curves at early times which becomes weaker at late times. All curves are obtained via a simulation using $q = 3$ and taking into account all processes to order $1/q^2$. The dashed red curve is the $q = \infty$ prediction for the functional form of the tail [Eq. (48)].

Let us now examine this OTOC in different regimes at late times such that the leading ballistic front is well separated from the diffusive “lump” near the origin: $\sqrt{D_c t} \ll v_B t$.

- (1) Outside the light cone $|x| > t$: Because of the locality of the circuit, a spreading operator $O_0(t)$ acts as the identity outside the light cone defined by $|x| \leq t$. Thus, the commutator $\mathcal{C}(x, t) = 0$ in this regime.
- (2) Beyond the leading operator fronts so $|x| \gg v_B t + \sqrt{D_c t}$, but within the causal light cone so $|x| < t$: Before the main operator front gets to x , any operator weight that is not locally the identity is exponentially small in t and thus the OTOC is also exponentially small in t (for fixed x/t in this regime). This regime does not exist for $q = \infty$. Reference [38] showed that the OTOC shows a near-exponential increase with time in this regime for the unconstrained circuit model, but with a position-dependent analog of the “Lyapunov exponent.” We expect the same qualitative behavior in this regime for our model, since this operator “edge” just comes from nonconserved

operators emitted at early times whose right and left weights then show biased diffusion, just as in the unconstrained circuit.

- (3) Within the leading operator fronts, $|x| - v_B t \sim \sqrt{D_\rho t}$: This regime describes the growth of the OTOC from an exponentially small value in t to an order 1 number due to the arrival of the ballistic front. Here, the operator right or left weight is again from nonconserved operators emitted at early times and, to leading order at long time for finite q , is a Gaussian of width $\sim \sqrt{D_\rho t}$, so the leading behavior of the OTOC in this regime is given by the corresponding error function that is the integral of this Gaussian profile, just as in the unconstrained circuit [37,38].
- (4) In the “tails,” $|x| \ll v_B t - \sqrt{D_\rho t}$: This regime describes the late-time approach of the OTOC to its final asymptotic value long after the main front has passed site x . In this regime, the deviation of the OTOC from its final value of one is given by the total weight (conserved and nonconserved) of operator strings that have not yet reached site x at time t . This is obtained by considering the total conserved weight at time $t' = (t - |x|/v_B)$, since any non-conserved fronts emitted after time t' do not reach site x by time t . Then, from Eqs. (47) and (21),

$$1 - C_{zr}^0(x, t) \approx \frac{1}{2\sqrt{\pi[t - (|x|/v_B)]}}. \quad (48)$$

Thus, the tails in the right and left weights of $z_0(t)$ lead to tails in the OTOC and, long after the front has passed site x , the OTOC still has a power law (in x and t) deficit from its asymptotic value. By contrast, in an unconstrained random circuit, the OTOC approaches 1 exponentially in time after the front passes. This slow power-law approach characterizes the diffusive tail in the late-time behavior of the OTOC. In the diffusive regime near the origin, $|x| \sim \sqrt{D_c t}$, there are further corrections to this of order $\sim 1/t$ from $\rho_c(x)$ that smoothly connect the OTOC's x dependence between $x < 0$ and $x > 0$.

Figure 5 shows a sketch of $C_{zr}^0(x, t)$ at different times, depicting the different regimes above.

B. OTOC between $r_0(t)$ and z_x

Let us now consider the OTOC between $r_0(t)$ and z_x , so that $\mu = 0$, $\alpha = 1 = r$, and $\beta = 3 = z$. Then,

$$C_{rz}^0(x, t) = 1 - \sum_{i < x} \rho_R(i, t) + \sum_{\substack{\text{strings } \mathcal{S}: \\ \text{rhs}(\mathcal{S}) \geq x \\ \mathcal{S}_x = (ra), (la)}} |a_{\mathcal{S}}^z|^2 - \sum_{\substack{\text{strings } \mathcal{S}: \\ \text{rhs}(\mathcal{S}) \geq x \\ \mathcal{S}_x = (la), (za)}} |a_{\mathcal{S}}^z|^2, \quad (49)$$

In this case, the first line is again sensitive to the overall operator shape, while the second line cares about the relative density difference within strings between local operators that are charged versus uncharged under \mathcal{R} , i.e., the difference in the local densities of r/l 's compared to \mathbb{I}/z 's—note that this is a different combination of local densities as compared to the one in Eq. (46).

Next, note that the average OTOC between $r_0(t)$ and z_x should equal the average OTOC between $z_0(t)$ and r_x since the two are related by time reversal: $C_{rz}^0(x, t) = C_{zr}^0(x, -t)$, and the average properties of our circuit are invariant under time reversal. In the previous section, we saw that the diffusive tail in the OTOC C_{zr}^0 Eq. (48) came from the tail in the right-weight profile of $z_0(t)$. However, recall from Sec. III B that the spreading $r_0(t)$ shows no tails in its ρ_R , since this operator starts out orthogonal to the conserved charges so that $\rho_R(x, t) \sim e^{-(x-v_B t)^2/4D_\rho t} / \sqrt{4\pi D_\rho t}$, and $\rho_R(x, t)$ is exponentially small for $x \ll v_B t$. Thus, the tail in C_{rz}^0 behind the ballistic front must come from the imbalance between the density of raising charges r/l and spin charges u/d (which are superpositions of \mathbb{I}/z). Indeed, we saw in Sec. IV that the coupling of spin and raising charge combined with the initial condition at the left and right fronts leads to a diffusive decay of the imbalance $\Delta_{\mathcal{R}_s}$ between the local ρ_r/ρ_l and ρ_u/ρ_d densities away from the locations of the fronts Eq. (42) (Fig. 4). Using Eq. (42), we find that the OTOC C_{rz}^0 in the regime $\sqrt{D_c t} \ll |x| \ll v_B t$ is given by $1 - C_{rz}^0(x, t) \approx \Delta_{\mathcal{R}_s}(x, t) \approx \{1/[2\sqrt{\pi(t - |x|/v_B)}]\}$, which agrees with Eq. (48), as it must.

This case provides a nice example of how the OTOC can probe the *internal* operator content inside the light cone and show diffusive tails, even when there are no tails in the overall operator shape of the spreading operator as measured by $\rho_{R/L}$.

C. OTOC between $z_0(t)$ and z_x

Turning next to the “diagonal” case $\mu = 0$, $\alpha = \beta = 3 = z$, we find that C_{zz}^0 has the same structure as in Eq. (49), but ρ_R now refers to the right-weight profile of $z_0(t)$. Thus, this commutator receives contributions *both* from the tails in the right weight and from the tails in the imbalance between the spin and raising charges, so that $1 - C_{zz}^0(x, t) \approx \{1/[\sqrt{\pi(t - |x|/v_B)}]\}$ for $|x| \ll v_B t$. Thus, a commutator between two conserved charges couples more strongly to the diffusive processes in the system, doubling the amplitude of the diffusive power-law tail in the OTOC, relative to the two other cases discussed above.

D. OTOC between $r_0(t)$ and r_x

Finally, consider the commutator between $r_0(t)$ and r_x so that $\alpha = \beta = 1$. Note that C_{rr}^0 has the same structure as in Eq. (46) [with ρ_R referring to the right weight of $r_0(t)$]. This commutator again shows a sharp increase when the ballistic

front reaches site x , but now *both* the contributions from the right weight and the “internal” operator content are exponentially suppressed away from the front so this OTOC does *not* show power-law tails in the regime $\sqrt{D_c t} \ll x \ll v_B t$ and approaches its asymptotic value exponentially after the front passes through. Instead, if we probe the commutator at short distances $x \sim \sqrt{D_c t}$, then the OTOC displays a weak effect within the diffusive cone from the diffusion of the initial raising charge, i.e., the diffusion of the imbalance between ρ_r and ρ_l . The same is true for OTOCs between $r(t)$ and l_x .

This result emphasizes that the diffusive tails in the OTOC at long distances and late times are tied to the operator dynamics of the conserved charges in the system. OTOCs between operators that are both orthogonal to the conserved charges do not display diffusive tails behind their fronts. Of course, if one simply measures the OTOC between two generic local operators, then these will have some overlap with the conserved charges and show diffusive tails.

E. $\mu \neq 0$

We now consider OTOCs evaluated in an equilibrium ensemble with a chemical potential $\mu > 0$ that weights different S_z^{tot} sectors, and we are interested in understanding the degree to which this compares with the finite-temperature OTOCs that have been evaluated for Hamiltonian models. A difference between the energy-conserving and S_z^{tot} -conserving cases is that, on the Hamiltonian side, both the Gibbs factor $e^{-\beta H}$ and the time evolution are governed by the same Hamiltonian. On the other hand, for the $U(1)$ problem, the “Gibbs factor” $e^{\mu N}$ commutes with the time-evolution operator $U(t)$ but is otherwise unrelated to it. This distinction between the two becomes important when considering nonzero μ .

To start, consider again the equilibrium Gibbs ensemble for a given chemical potential:

$$\begin{aligned} \rho_\mu^{\text{eq}} &= \frac{e^{\mu S_z^{\text{tot}}}}{\text{Tr} e^{\mu S_z^{\text{tot}}}} = \prod_{i=1}^L \frac{1 + z_i \tanh \mu}{2q} \\ &= \prod_{i=1}^L \frac{1}{2q} \left[u_i \left(\frac{1 + \tanh \mu}{\sqrt{2}} \right) + d_i \left(\frac{1 - \tanh \mu}{\sqrt{2}} \right) \right], \end{aligned} \quad (50)$$

where we have switched to the (normalized) u/d basis which projects onto up and down conserved spins in the last line. In the limit $\mu \rightarrow \infty$,

$$\rho_\infty^{\text{eq}} = (2q)^{-L} \prod_i (\sqrt{2} u_i) = q^{-L} \prod_i (|\uparrow\rangle\langle\uparrow| \otimes \mathbb{I})_i. \quad (51)$$

In this limit, ρ_∞^{eq} projects the conserved spins to the “all up” state so that the conserved part of the dynamics is completely “frozen out,” reducing the system to just the

unconstrained qudit spins. The unconstrained qudit system is chaotic and displays ballistic growth of operators with a nonzero q -dependent butterfly velocity, just as in the unconstrained random circuit model [37,38]. This illustrates how the independence of $U(t)$ and ρ^{eq} can lead to chaotic dynamics even in the $\mu \rightarrow \infty$ limit, while the analogous $T \rightarrow 0$ limit for Hamiltonian systems arrests chaos. On the other hand, if one considers $\mu \rightarrow \infty$ with $q = 1$, then the butterfly speed does go to zero since spin flips in this fully polarized background can move at most diffusively. Thus, the $q = 1$ problem as $\mu \rightarrow \infty$ is closer to the zero-temperature dynamics of Hamiltonian systems. In the rest of this section, we work at $q = 1$ in the $\mu \rightarrow \infty$ limit.

We start with $\mu = \infty$ where ρ_∞^{eq} reduces to the projector on the $|0\rangle \equiv |\uparrow\uparrow\cdots\uparrow\rangle$ state. Then,

$$C_{\alpha\beta}^\infty = \frac{1}{2} \langle 0 | [|\sigma_0^\alpha(t), \sigma_x^\beta\rangle]^2 | 0 \rangle. \quad (52)$$

First consider OTOCs involving z and r . Since $|0\rangle$ is an eigenstate of both r and z (with eigenvalues 0 and 1, respectively), any commutator involving only r 's or z 's must be strictly zero. Thus, the only nontrivial OTOCs are those involving $[l_0(t), z_x]$ and $[l_0(t), r_x]$ (the commutators between $[z_0(t), l_x]$ and $[r_0(t), l_x]$ will be related to these by time reversal). Let us start with $C_{l_z}^\infty$. Expanding the commutator, we find

$$\begin{aligned} C_{l_z}^\infty &= \frac{1}{2} \langle 0 | [l_0(t), z_x]^2 | 0 \rangle \\ &= \frac{1}{2} \langle 0 | [z_x r_0(t) - r_0(t) z_x] [l_0(t) z_x - z_x l_0(t)] | 0 \rangle \\ &= 2 - \langle 0 | r_0(t) z_x l_0(t) | 0 \rangle, \end{aligned} \quad (53)$$

where we have made use of the fact that $|0\rangle$ is an eigenstate of $U(t)$, z and $r_0 l_0$ in the last line, with eigenvalues 1, 1, and 2, respectively. Now, every basis string that appears in the operator expansion of $l_0(t)$ has net raising charge $\mathcal{R}^{\text{tot}} = -1$. Since $|0\rangle$ is annihilated by any r_i , all strings in the expansion of $l_0(t)$ that contain r 's cannot contribute to the OTOC, and thus only strings containing exactly one l_i on some site (with arbitrary \mathbb{I} 's and z 's on the others) can contribute. These create single spin flips in the polarized background. Of these, only the strings which contain l_x fail to commute with z_x . However, due to the diffusion of raising charge \mathcal{R}_i discussed in Sec. IV, the weight of the operator on such “single l ” strings decays only diffusively away from the origin, showing that this OTOC displays only diffusive (as opposed to ballistic) behavior corresponding to a zero butterfly speed. Likewise, consider the infinite μ OTOC involving $[l_0(t), r_x]$:

$$\begin{aligned}
C_{lr}^\infty &= \frac{1}{2} \langle 0 | [l_0(t), r_x]^2 | 0 \rangle \\
&= \frac{1}{2} \langle 0 | r_0(t) (l_x r_x) l_0(t) | 0 \rangle \\
&= \frac{1}{2} - \frac{1}{2} \langle 0 | r_0(t) z_x l_0(t) | 0 \rangle, \tag{54}
\end{aligned}$$

where we have made use of the fact that $r_x | 0 \rangle = \langle 0 | l_x = 0$, and $(lr) = (1 - z)$. Thus, this OTOC has an identical structure to Eq. (53) and also displays purely diffusive behavior. Perturbing ρ_μ^∞ away from $\mu = \infty$ to leading order in large but not infinite μ gives [Eq. (50)]

$$\rho_{\mu \rightarrow \infty}^{\text{eq}} \approx (2)^{-L} \prod_i \sqrt{2} [(1 - e^{-2\mu}) u_i + e^{-2\mu} d_i]. \tag{55}$$

Understanding the modifications to the diffusive $\mu = \infty$ behavior of the OTOCs at large but finite μ is an interesting question that has been explored in detail in Ref. [54].

VI. PHYSICAL SYSTEMS

Let us now turn to more generic examples of thermalizing spin chains with conservation laws, and examine to what extent the universal aspects of our results continue to hold in this setting. Since analytic results for the dynamics are not easily obtained for these systems, we will study them numerically using exact diagonalization. We will first look at a periodically driven ‘‘Floquet’’ spin chain where energy is not conserved, but S_z^{tot} is, just like in our random circuit model. We then turn to a interacting quantum chaotic spin chain with energy conservation.

A. S_z^{tot} -conserving Floquet chain

We consider a one-dimensional chain of spin-1/2 qubits that is periodically driven in time with period τ between two separate Hamiltonians H_z and H_{xy} , each of which act for half the period. The time-evolution operator for this system is

$$U_F(\tau) = e^{i(\tau/2)H_z} e^{i(\tau/2)H_{xy}}, \tag{56}$$

with

$$\begin{aligned}
H_z &= J_z \sum_i \sigma_i^z \sigma_{i+1}^z, \\
H_{xy} &= \sum_i [J_x \sigma_i^x \sigma_{i+1}^x + J_y \sigma_i^y \sigma_{i+1}^y]. \tag{57}
\end{aligned}$$

The parameters we choose for this model are $J_z = (10 + \sqrt{5})/16$, $J_x = J_y = (5 + 5\sqrt{5})/16$, and $\tau = 1$, where we have found numerically that this system is well thermalizing, even though the individual Hamiltonians in the drive are integrable [55]. The time evolution conserves total S_z^{tot} : $[U(\tau), S_z^{\text{tot}}] = 0$ and, just as in the random circuit

problem, operators like r/l have a definite ΔS_z^{tot} action which is respected by the time evolution. We will measure time discretely in multiples of τ , and the time evolution of operators in the Heisenberg picture is given by $O(n\tau) = U_F^\dagger(n\tau) O(0) U_F(n\tau)$. Finally, there is no randomness in this problem, and the time evolution respects locality.

Of course, the fact that charges in this thermalizing model will display diffusive dynamics is well understood. We wish to probe the interaction between the diffusive charge dynamics and the ballistic operator growth, say, as probed through the right-weight profiles $\rho_R(x, t)$ of $r_0(t)$ and $z_0(t)$. While ρ_R for $z(t)$ does show a tail for this model, it is difficult to tease apart the different regimes for small finite-sized systems accessible to exact-diagonalization studies (it only takes time $t \sim L^2$ for the diffusive charges to reach the end of the chain). To aid with this, we consider a related quantity, the ℓ weight $W_\ell(x, t)$, which measures the weight on all Pauli strings with maximum end-to-end separation between nonidentity elements equal to x :

$$W_\ell(x, t) = \sum_{\substack{\mathcal{S}: \text{lhs}(\mathcal{S}) - \\ \text{rhs}(\mathcal{S}) = x}} |a_{\mathcal{S}}|^2, \tag{58}$$

where, as before, the lhs and rhs of \mathcal{S} define the locations of the rightmost and leftmost nonidentity operators in \mathcal{S} . This has the advantage that all conserved charges have the form z_i and these are all mapped to $x = 0$. On the other hand, strings that are part of the ballistic front and stretched between $-v_B t$, $v_B t$ contribute to $x = 2v_B t$. Thus, the nonconserved contributions to this quantity still show ballistic dynamics. In a system with no conservation laws, $W_\ell(x, t)$ for $x < v_B t$ decays exponentially with t and quickly approaches its asymptotic value which is itself exponentially small in L . On the other hand, in a system with conservation laws, this quantity decays as a power law and approaches its asymptotic value which is instead only power law small in L if one starts with an initial operator which has overlap with the conserved densities (at late times, each conserved amplitude $\sim 1/L$, so that the total weight on all conserved charges is $\sim L/L^2 = 1/L$). This helps us tease apart the dynamics of the conserved charge at these small sizes.

Figure 6 shows the ℓ -weight profiles $W_\ell(x, t)$ for both $r_0(t)$ and $z_0(t)$ for a 12-site chain, with both operators starting at the end of the chain to maximize the available distance for spreading. We clearly see the tail and ‘‘lump’’ with enhanced ℓ weight at $x = 0$ for $z_0(t)$. On the other hand, the late-time profile for $r_0(t)$ shows a simple decay of the ℓ weight, with the most weight on strings stretched across the entire system, i.e., those with $x = L$. These data show that the central aspects of our results on operator shape seem to be born out for this more ‘‘physical’’ spin chain, although for such a short chain this can only be qualitatively tested in the numerics.

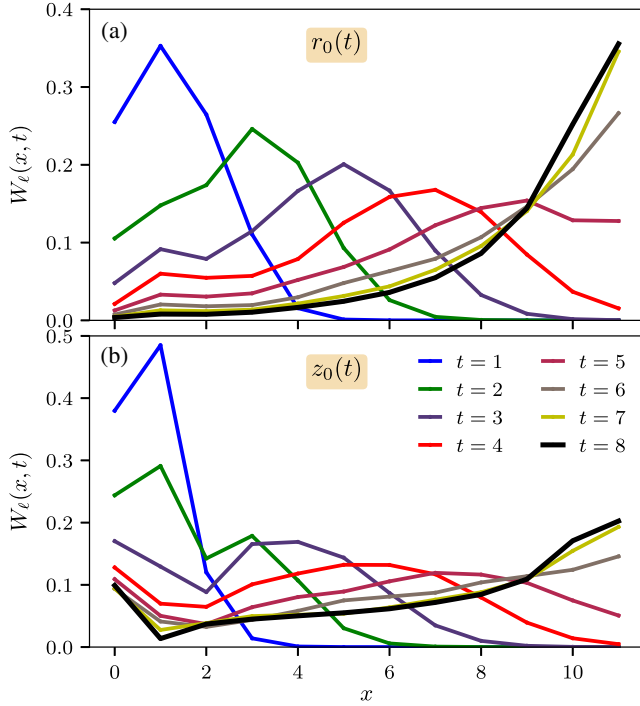


FIG. 6. ℓ -weight profile $W_\ell(x, t)$ Eq. (58) of spreading operators $z_0(t)$ and $r_0(t)$ in a Floquet model that conserves S_z^{tot} Eq. (57), plotted for a system of length $L = 12$. The expected diffusive “lump” in the right-weight profile of the spreading conserved charge is manifested in the enhanced weight of $W_\ell(x, t)$ at $x = 0$ for $z_0(t)$, even at late times (b). No such enhancement is observed for $r_0(t)$ which evolves orthogonal to the conserved charges (a). Notice also that the late-time decay of $W_\ell(x, t)$ away from $x = L$ is much slower for $z_0(t)$ as compared to $r_0(t)$, consistent with the presence of power-law diffusive tails in the right-weight profile of the former but not the latter.

B. Hamiltonian spin chain

We now turn to a thermalizing Hamiltonian spin chain with energy conservation, but no other continuous symmetries [43]:

$$H = \sum_i J \sigma_i^z \sigma_{i+1}^z + h_x \sigma_i^x + h_z \sigma_i^z, \quad (59)$$

where $J = 1$, $h_x = (\sqrt{5} + 5)/8$, $h_z = (\sqrt{5} + 1)/4$. The local energy density operators are one- and two-site Pauli strings of the form σ_i^x , σ_i^z , and $\sigma_i^z \sigma_{i+1}^z$. The conservation of total energy implies that $\text{Tr}[O_0(t)H] = \text{const}$, and thus, if we start with an operator with a nonzero overlap with a local energy density, then the sum of the amplitudes of the spreading operator on all the local energy density strings is conserved. A difference between this Hamiltonian model and the $U(1)$ conserving model is that energy is not quantized and there are no special operators (like r) with definite algebras under H . Even if we start with a local operator that is orthogonal to all the conserved energy

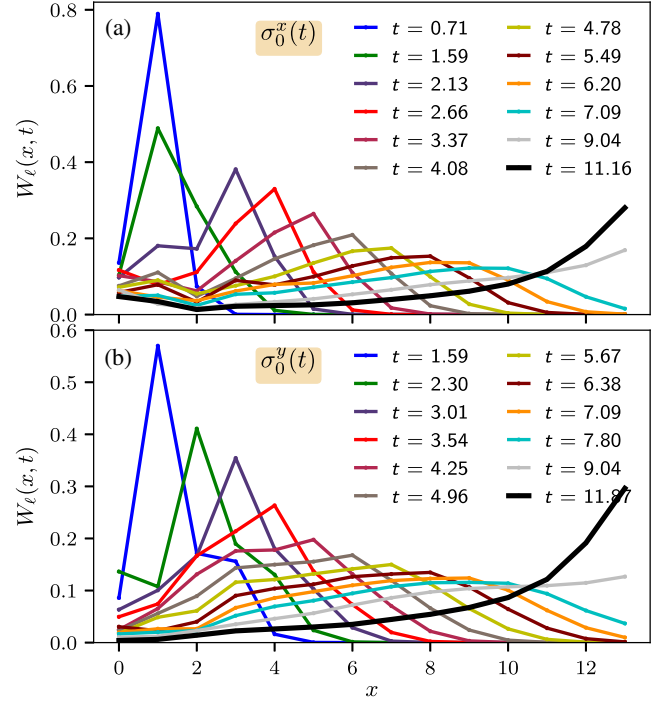


FIG. 7. ℓ -weight profile $W_\ell(x, t)$ Eq. (58) of spreading operators $\sigma_0^x(t)$ and $\sigma_0^y(t)$ in a thermalizing Hamiltonian model that conserves energy Eq. (59), plotted for a system of length $L = 14$. σ_0^y has nontrivial overlap with the local conserved energy density operators, which is visible in the enhanced weight of $W_\ell(x, t)$ for $x = 0, 1$ even at late times (a). By contrast, σ_0^x starts out orthogonal to the conserved charges and its late-time ℓ -weight profile does not show a “lump” at $x = 0, 1$. While the late-time decay of $W_\ell(x, t)$ away from $x = L$ is again faster for $\sigma_0^y(t)$ as compared to $\sigma_0^x(t)$, the difference is not as pronounced as the difference between $z_0(t)$ and $r_0(t)$ in the $U(1)$ Floquet case. This is because $\sigma_0^y(t)$ can develop overlap with the slow conserved charges, unlike $r_0(t)$ which is constrained to remain strictly orthogonal to the charges during its entire evolution.

densities (like σ_i^y), its operator expansion will, in time, develop some overlaps with the conserved charges.

Figure 7 shows the ℓ -weight profile for the spreading of $\sigma_0^x(t)$ and $\sigma_0^y(t)$ in a system of length $L = 14$ obtained using exact diagonalization and, once again, we see the lump at $x = 0, 1$ only in the former. Notice, however, that the difference between σ_0^x and σ_0^y in the decay of $W_\ell(x, t)$ away from $x = L$ at late times is not as pronounced as it is in the Floquet problem (Fig. 6). We attribute this to the fact that the time-evolving $\sigma_0^y(t)$ develops nontrivial overlap with the diffusing conserved charges (even though the sum of the amplitudes on all conserved charges is constrained to be zero), slowing down its dynamics relative to $r_0(t)$ in the Floquet model, which always evolves strictly orthogonal to the conserved charges. This is one example of a difference between $U(1)$ conservation with quantized charges and energy conservation where the charges are continuous.

As discussed in the previous section, these power-law tails in operator shape translate into power-law tails in the long-distance and late-time OTOC, and these have been observed numerically in Hamiltonian systems with conservation laws [41].

VII. CONCLUSIONS

In conclusion, we present an extensive study of the “scrambling” dynamics of local operators in chaotic quantum systems with a conserved, diffusing charge (or energy) density. A generic local operator in this setting has some weight on the conserved charges, and the late-time spreading dynamics of such an operator is described by multiple coupled hydrodynamic processes. The first is the “physical” hydrodynamics associated with the diffusive dynamics of the conserved charges. We show that the total operator weight on these conserved charges decreases as power law in time which, by unitarity, necessitates a steady “emission” process that transfers operator weight from local conserved densities to nonconserved operators. This emission happens at a slow hydrodynamic rate set by the local diffusive currents of the conserved density but, once emitted, the fronts of the nonconserved operators spread ballistically and rapidly become nonlocal. The propagation of the nonconserved fronts is described via an “emergent hydrodynamics” that is biased diffusion for the one-dimensional case [37,38], and this coupled diffusion-emission-propagation process reveals a composite picture for the operator profile, showing how the ballistic and diffusive processes in the system connect at different timescales and length scales. In particular, the presence of slow diffusive modes leads to the development of a power-law tail in the operator profile that reflects the weight of nonconserved operator strings emitted at later times that “lag” behind the leading ballistic front.

Our picture illustrates how reversible unitary dynamics in closed quantum systems can display dissipative diffusive hydrodynamic modes. The dissipation arises from the conversion of operator weight from locally observable conserved parts to nonlocal nonconserved parts at a slow hydrodynamic rate, a process which increases the “observable” entropy of the system. By contrast, in systems without conservation laws, any local operator is rapidly converted to nonlocal, so the dissipation does not appear in the late-time hydrodynamics of operator or entanglement spreading.

In addition to the diffusive tails in the distribution of operator weight, we find an additional layer of structure describing the local operator content behind the ballistic front, *within* the spreading operator. Outside the ballistic operator front, the spreading operator locally consists only of local identities. The arrival of the front at a given site turns on a noisy coupled diffusion process between different species of local operators, which relaxes the initially imbalanced local operator content to the final equilibrium

value where all local operators are equally likely. Once again, this relaxation happens at a power law slow rate and contributes to the operator hydrodynamics, in contrast to the unconstrained random circuit case where the action of a single gate at the front erases the initial bias towards the identities. These power-law tails in the distributions of operator weight and local operator content also lead to diffusive tails in the late-time approach of certain out-of-time-order commutators to their asymptotic values.

In all, our work reveals several rich layers of physics in the scrambling dynamics of systems with conservation laws. We expect this approach (which builds on work by Refs [36–38]) of probing the dynamics of such systems via an analytically tractable constrained random unitary circuits will have broader applicability in understanding the many open questions about the fundamentals of thermalization and quantum statistical mechanics in chaotic quantum systems with conservation laws. It would also be interesting to ask which of our results can also be calculated (or extended) in a holographic setting, where they might connect with the dynamics of black holes with charges.

Recently, we became aware of related work by Rakovszky *et al.* [54]. While these authors take a somewhat different approach, our results appear to agree where they overlap.

ACKNOWLEDGMENTS

We thank Cheryne Jonay, Joel Lebowitz, Adam Nahum, Stephen Shenker, Shivaji Sondhi, Douglas Stanford, and Brian Swingle for helpful discussions. V. K. was supported by the Harvard Society of Fellows and the William F. Milton Fund. A.V. was supported by a Simons Investigator grant.

APPENDIX A: ACTION OF S_z^{tot} -CONSERVING UNITARY ON DIFFERENT OPERATORS

There are a few classes of operators on site i that evolve differently under the action of U . These are $(ra)_i$, $(la)_i$, $(z\mathbb{I})_i$, $(zn)_i$, $(\mathbb{III})_i$, and $(\mathbb{II}n)_i$. We use the labels $a = \text{“any”}$ and $n = \text{“nonidentity”}$ to refer to the set of qudit operators that take any value or that act as the nonidentity, respectively. If one starts with an operator with a definite action (such as “raise by one”) under the $U(1)$ symmetry, the circuit preserves this action. The action of $U_{i,i+1}$ on two-site operators can be summarized as follows (in all cases the norm of the operator is preserved).

- (1) The operators $(\mathbb{III})_i(\mathbb{III})_{i+1}$, $(z\mathbb{I})_i(z\mathbb{I})_{i+1}$, and $[(z\mathbb{I})_i(\mathbb{III})_{i+1} + (\mathbb{III})_i(z\mathbb{I})_{i+1}]/\sqrt{2}$ are invariant under the action of the gate due to the conservation law.
- (2) The $4q^4$ raise-by-one operators $(ra)_i(\mathbb{I}a)_{i+1}$, $(ra)_i(za)_{i+1}$, $(\mathbb{I}a)_i(ra)_{i+1}$, and $(za)_i(ra)_{i+1}$ each transition to a uniformly random linear combination of these operators. Similarly, the lower-by-one operators $(la)_i(\mathbb{I}a)_{i+1}$, $(la)_i(za)_{i+1}$, $(\mathbb{I}a)_i(la)_{i+1}$,

- and $(za)_i(la)_{i+1}$ each transition to a uniformly random linear combination of these $4q^4$ operators.
- (3) The q^4 raise-by-two operators $(ra)_i(ra)_{i+1}$ each transition to a uniformly random linear combination of these operators. Likewise, the lower-by-two operators $(la)_i(la)_{i+1}$ each transition to uniformly a random linear combination of these q^4 operators.
- (4) The $(6q^4 - 3) S_z^{\text{tot}}$ -conserving operators $(ra)_i(la)_{i+1}$, $(la)_i(ra)_{i+1}$, $(\mathbb{I}a)_i(\mathbb{I}a)_{i+1}$, $(za)_i(za)_{i+1}$, $(\mathbb{I}a)_i(za)_{i+1}$, and $(za)_i(\mathbb{I}a)_{i+1}$ (excluding the three special operators in case 1 above) each transition to a random linear combination of these operators, but here with nonuniform probabilities. This is due to the fact that the \mathbb{I} 's and z 's are superpositions of the conserved up and down spin charges introduced in Sec. IV.

Thus, it is more convenient to express these transitions directly in terms of the up and down qubit projection operators $u = [(\mathbb{I} + z)/\sqrt{2}]$ and $d = [(\mathbb{I} - z)/\sqrt{2}]$:

- (a) $(u\mathbb{I})_i(u\mathbb{I})_{i+1}$, $(d\mathbb{I})_i(d\mathbb{I})_{i+1}$, and $[(u\mathbb{I})_i(d\mathbb{I})_{i+1} + (d\mathbb{I})_i(u\mathbb{I})_{i+1}]/\sqrt{2}$ are left invariant by the action of the circuit.
- (b) The $(q^4 - 1)$ operators $(ua)_i(ua)_{i+1}$ [but not including the conserved $(u\mathbb{I})_i(u\mathbb{I})_{i+1}$] each transition to a uniformly random linear combination of these operators.
- (c) Likewise, the $(q^4 - 1)$ operators $(da)_i(da)_{i+1}$ [but not including the conserved $(d\mathbb{I})_i(d\mathbb{I})_{i+1}$] each transition to a uniformly random linear combination of these operators.
- (d) The $(4q^4 - 1)$ operators $(ra)_i(la)_{i+1}$, $(la)_i(ra)_{i+1}$, $(ua)_i(da)_{i+1}$, and $(da)_i(ua)_{i+1}$ [not including the conserved $[(u\mathbb{I})_i(d\mathbb{I})_{i+1} + (d\mathbb{I})_i(u\mathbb{I})_{i+1}]/\sqrt{2}$] each transition to a uniformly random linear combination of these operators.

Finally, for completeness, we note that the raise- or lower-by-one operators in case (2) above split into two groups each in the u, d basis:

- (a) The $2q^4$ operators of the form $(ra)_i(ua)_{i+1}$, $(ua)_i(ra)_{i+1}$ mix between each other with equal probability $1/2q^4$. These act on states (on this two site subspace) with $S_z^{\text{tot}} = 0$ and produce states with $S_z^{\text{tot}} = 1$.
- (b) The $2q^4$ operators of the form $(ra)_i(da)_{i+1}$, $(da)_i(ra)_{i+1}$ mix between each other with equal probability $1/2q^4$. These act on states (on this two site subspace) with $S_z^{\text{tot}} = -2$ and produce states with $S_z^{\text{tot}} = -1$.
- (c) The $2q^4$ operators of the form $(la)_i(ua)_{i+1}$, $(ua)_i(la)_{i+1}$ mix between each other with equal probability $1/2q^4$. These act on states (on this two site subspace) with $S_z^{\text{tot}} = 2$ and produce states with $S_z^{\text{tot}} = 1$.

- (d) The $2q^4$ operators of the form $(la)_i(da)_{i+1}$, $(da)_i(la)_{i+1}$ mix between each other with equal probability $1/2q^4$. These act on states (on this two site subspace) with $S_z^{\text{tot}} = 0$ and produce states with $S_z^{\text{tot}} = -1$.

Note that in the u, d, r, l basis, the action of the circuit looks symmetric with respect to interchanging $r \leftrightarrow l$ and $u \leftrightarrow d$.

APPENDIX B: DERIVATION OF THE BUTTERFLY SPEED v_B AND THE DIFFUSION CONSTANT D_ρ TO $O(1/q^2)$

In this appendix, we derive the butterfly speed v_B and the diffusion constant D_ρ characterizing the biased diffusion of the nonconserved operator fronts. We assume we are working at late times, so the ballistic front of nonconserved operators is well separated from the diffusive lump of conserved charges near the origin. We present the discussion below for the propagation of the right front, but the same holds for the left front as well, just reflected.

We find it convenient to define the right front of an operator string as the location of the rightmost two-site unitary gate that sees a nonidentity operator at time t . So, for instance, if an operator string ends on site i at time t , the front (for this string) is either between sites $(i, i+1)$ or between sites $(i-1, i)$, depending on the evenness and oddness of t, i due to the even-odd staggered structure of the circuit (Fig. 1). Without loss of generality, let us consider a particular operator string for which the front at time t is at the gate on sites $(i, i+1)$. Now, under the action of the circuit, the front gate has a probability that is suppressed as $O(1/q^2)$ for creating $(\mathbb{I}\mathbb{I})_{i+1}$ on site $(i+1)$ (Appendix A) [unless the string's local operators at the front gate are $(z\mathbb{I})_i(\mathbb{I}\mathbb{I})_{i+1}$, $(\mathbb{I}\mathbb{I})_i(z\mathbb{I})_{i+1}$ or $(z\mathbb{I})_i(z\mathbb{I})_{i+1}$; we return to these cases below, which are themselves suppressed in probability by $O(1/q^2)$, $O(1/q^4)$, and $O(1/q^4)$, respectively]. When the front gate creates an identity on site $(i+1)$, the string ends on site i at time $(t+1)$. But, due to the even-odd staggering of gates, this means that the front at time $(t+1)$ is on the sites $(i-1, i)$, which means it moved *back* one step. On the other hand, if the front gate at time t produces a nonidentity on site $(i+1)$ [which happens with probability $1 - O(1/q^2)$], then the front at time $(t+1)$ is on sites $(i+1, i+2)$, which means it moves forward one step. At $q = \infty$, the front deterministically moves forward at every time step which gives a butterfly velocity $v_B = 1$. Also, in this limit, the front of the full initially local operator remains perfectly sharp since there is no probabilistic spread in the locations of the fronts of the strings that make up the resulting spreading operator.

We now estimate the leading $1/q^2$ correction to the butterfly speed. To do this, we need to estimate the probability of the front moving backward. Note that the most probable configuration of local operators on the front

gate takes the form $(n)_i(\mathbb{I})_{i+1}$, where n is a nonidentity. This is because if the action of the front gate $(i-1, i)$ at time $(t-1)$ produces a nonidentity on site i (which is the most probable option at large q), then this nonidentity meets the identity on site $(i+1)$ on the front gate at the next time step, which is at $(i, i+1)$. The different types of front operators that belong to this category are (i) $(ra)_i(\mathbb{I})_{i+1}$, (ii) $(la)_i(\mathbb{I})_{i+1}$, (iii) $(\mathbb{I}n)_i(\mathbb{I})_{i+1}$, (iv) $(zn)_i(\mathbb{I})_{i+1}$, and (v) $(z\mathbb{I})_i(\mathbb{I})_{i+1}$, where we have split the z case into two for reasons that will become clear momentarily. To estimate the probability of the front moving backward, we need to estimate the steady-state probability of getting these different operator types at the front, and the probability of the different types moving back. We will find that cases (i)–(iv) exist with $O(1)$ probabilities and move back with probability $O(1/q^2)$, while case (v) exists with probability $(1/q^2)$ and moves back with probability $O(1)$. Thus, each of these gives an $O(1/q^2)$ probability of moving backward. Note that we do not need to consider front operators of the form $(a)_i(n)_{i+1}$ at this order, because the only way to produce front operators of this form is for the front to have moved backward at the previous step $(t-1)$, i.e., the front at $(t-1)$ was at sites $(i+1, i+2)$ and created an identity on site $(i+2)$ leading to the front moving to sites $(i, i+1)$ at time t , where the nonidentity on site $(i+1)$ now generically meets a nonidentity on the “backward” site i with probability $O(1-1/q^2)$. Thus, the front gate sees motifs like $(n)_i(n)_{i+1}$ with probability $O(1/q^2)$ and they move back with probability $O(1/q^2)$, thereby giving a higher-order $O(1/q^4)$ correction to v_B . The case where the front sees $(\mathbb{I})_i(z\mathbb{I})_{i+1}$ is further reduced by a factor of $1/q^2$ since this case requires both the front to move back at the previous time step and for the qudit operator on site i to be the identity.

We now turn to the steady-state probabilities of the different operator types (i)–(v) at the front. Since we only need the probabilities for (i)–(iv) correct to $O(1)$, we can estimate them at infinite q . The infinite q answer for Δ_{rs} Eq. (41) evaluated at the location of the front $x=t$, combined with the fact that $\rho_r = \rho_l$ and $\rho_u = \rho_d$ at the front, tells us that, at infinite q , the front gate looks like $(ra)_i(\mathbb{I})_{i+1}$ or $(la)_i(\mathbb{I})_{i+1}$ with equal probability $1/6$, and it looks like $(un)_i(\mathbb{I})_{i+1}$ or $(dn)_i(\mathbb{I})_{i+1}$ with probability $1/3$. The latter two cases translate to an equal $1/3$ probability for obtaining $(zn)_i(\mathbb{I})_{i+1}$ and $(\mathbb{I}n)_i(\mathbb{I})_{i+1}$ at the front gate. On the other hand, the probability for seeing a $(z\mathbb{I})_i(\mathbb{I})_{i+1}$ at the gate is only $O(1/q^2)$. This is because, away from the location of the diffusing charges, processes that generate such an operator at a site have q^2 choices for the operator on the qudit spin, and an \mathbb{I} on the qudit spin reflects only one of these q^2 choices. Thus, we denote the probability of obtaining $(z\mathbb{I})_i(\mathbb{I})_{i+1}$ at the front as (p_z/q^2) , and self-consistently solve for p_z below.

- (1) The input to the last gate is $(ra)_i(\mathbb{I})_{i+1}$ or $(la)_i(\mathbb{I})_{i+1}$ with equal probability $1/6 + O(1/q^2)$.

These produce a $(\mathbb{I})_{i+1}$ on site $(i+1)$ with probability $1/(4q^2)$ (Appendix A), which makes the front move back. Or they produce $[(z\mathbb{I})_{i+1}]$ on site $(i+1)$ with probability $1/(4q^2)$, which results in the front gate at the time $(t+1)$ seeing the operator $(z\mathbb{I})_i(\mathbb{I})_{i+1}$.

- (2) With probability $2/3 + O(1/q^2)$, the last gate gets input $(zn)_i(\mathbb{I})_{i+1}$ or $(\mathbb{I}n)_i(\mathbb{I})_{i+1}$. These are either $(un)(u\mathbb{I})$, $(dn)(d\mathbb{I})$, $(un)(d\mathbb{I})$, or $(dn)(u\mathbb{I})$ with equal probabilities, where we have expressed the qubit operators z and \mathbb{I} as a superposition of u and d . Now, under the action of the circuit, $(un)(u\mathbb{I})$ transforms into a uniformly random linear combination of all $(ua)(ua)$ except $(u\mathbb{I})(u\mathbb{I})$, and $(dn)(d\mathbb{I})$ does likewise (Appendix A). Thus, these only make z and \mathbb{I} qubit operators at these two sites. On the other hand, $(un)(d\mathbb{I})$, $(dn)(u\mathbb{I})$ equally make all four qubit operator types (r, l, z, \mathbb{I}) , since these mix between $(ra)_i(la)_{i+1}$, $(la)_i(ra)_{i+1}$, $(ua)_i(da)_{i+1}$, and $(da)_i(ua)_{i+1}$ with equal probability to order $1/q^2$. As a result, given this input, the outputs on qubits are \mathbb{I} 's with probability $3/8$, z 's with probability $3/8$, and otherwise r 's or l 's. So for these cases the resulting output on the front site $(i+1)$ is $(\mathbb{I})_{i+1}$ with probability $3/(8q^2)$, and this results in the front moving backward. Similarly, the resulting output on the front site is $(z\mathbb{I})_{i+1}$ with probability $3/(8q^2)$, which results in the front gate at the time $(t+1)$ seeing the operator $(z\mathbb{I})_i(\mathbb{I})_{i+1}$.
- (3) Finally, with probability p_z/q^2 the last gate gets input $(z\mathbb{I})_i(\mathbb{I})_{i+1}$ (where p_z/q^2 is a steady-state probability yet to be determined). With probability $1/4 + O(1/q^2)$ this is left alone, so the front moves back. Or the resulting output on the front site is $(z\mathbb{I})_{i+1}$ with probability $(1/4 + O(1/q^2))$. This follows since $(z\mathbb{I})_i(\mathbb{I})_{i+1} = \{[(z\mathbb{I})_i(\mathbb{I})_{i+1} + (\mathbb{I})_i(z\mathbb{I})_{i+1}]/2\} + \{[(z\mathbb{I})_i(\mathbb{I})_{i+1} - (\mathbb{I})_i(z\mathbb{I})_{i+1}]/2\}$, and the former is conserved under the action of the circuit while the latter mixes between q^4 different operators. The conservation of the former gives the leading $1/4$ probability for producing $(z\mathbb{I})_i$ or $(z\mathbb{I})_{i+1}$.

We can now use (i)–(iii) to self-consistently solve for the steady-state value of p_z at the front:

$$\frac{p_z}{q^2}(t+1) = \frac{1}{4q^2} \frac{2}{6} + \frac{3}{8q^2} \frac{2}{3} + \frac{1}{4} \frac{p_z}{q^2}(t) = \frac{p_z}{q^2}(t),$$

where the last equality is true in the steady state. Solving this gives $p_z = 4/9$. Finally, putting together the probability of each operator type at the front with the probability for a given type to move back gives a net probability for the front to move back equal to $p_{\text{backward}} = 4/9q^2$, which means the butterfly velocity is $v_B = (p_{\text{forward}} - p_{\text{backward}}) = 1 - 8/(9q^2)$.

Next, we estimate the diffusion constant for the biased random walk of the operator front. After t steps, the expectation value of the location of the front is denoted $\langle X \rangle_t = \langle \sum_{i=1}^t x_i \rangle$, where $x_i = -1$ with probability p_{backward} and $x_i = +1$ with probability $1 - p_{\text{backward}}$. Then,

$$\begin{aligned} \Delta_X &\equiv \left\langle \left(\sum_{i=1}^t x_i \right)^2 \right\rangle - \left\langle \sum_{i=1}^t x_i \right\rangle^2 \\ &= t + \left\langle \sum_{i \neq j} x_i x_j \right\rangle - (v_B t)^2. \end{aligned}$$

Unlike a Markovian random walk where x_i and x_j at different time steps are independent, the constrained action of the circuit does introduce correlations between x_i and x_j . However, these appear only at $O(1/q^4)$ and higher. To see this, one can look at the modified probabilities of the front operators at time t given that the front moved forward or backward at time $t-1$ (and other such processes), and we find that all of these only receive higher-order corrections at $1/q^4$. Thus, to leading order in $1/q^2$, the random walk does look Markovian, which gives a diffusion constant equal to $D_\rho = (1 - v_B^2)/2 \approx 8/(9q^2)$.

APPENDIX C: AMPLITUDES AND WEIGHTS OF THE EVOLVING OPERATOR ON THE CONSERVED DENSITIES

To see the evolution of the conserved amplitudes $a_i^c(t)$ under the unitary dynamics, consider the action of the gate U_{12} on $[a_1^c(z\mathbb{I})_1 + a_2^c(z\mathbb{I})_2]$:

$$\begin{aligned} a_1^c(z\mathbb{I})_1 + a_2^c(z\mathbb{I})_2 &= (a_1^c + a_2^c) \left[\frac{(z\mathbb{I})_1(\mathbb{III})_2 + (\mathbb{III})_1(z\mathbb{I})_2}{2} \right] \\ &\quad + (a_1^c - a_2^c) \left[\frac{(z\mathbb{I})_1(\mathbb{III})_2 - (\mathbb{III})_1(z\mathbb{I})_2}{2} \right]. \end{aligned} \quad (\text{C1})$$

The first term above is unchanged under the action of U_{12} , and the second term is a nonconserved operator since its net overlap with S_z^{tot} is zero. Under the action of U_{12} , the second term transitions to a random superposition of order q^4 operators that locally conserve S_z^{tot} but act arbitrarily on the qudit (Appendix A). Only one of these operators—corresponding to the second term returning to itself—contributes to the amplitudes of the conserved charges. The amplitude for this term is of order $1/q^2$, but it is random and vanishes upon averaging over different random circuits. Thus, after the action of the gate, the Haar-averaged amplitude of the conserved local operator on both outgoing sites is equal to the average of the incoming amplitudes:

$$\overline{a_1^c(t+1)} = \overline{a_2^c(t+1)} = \frac{\overline{a_1^c(t)} + \overline{a_2^c(t)}}{2}. \quad (\text{C2})$$

Starting with $(z\mathbb{I})_0$ on a single site and recursively applying this formula gives a “doubled” version of Pascal’s triangle (due to the even-odd structure of the circuit) according to which the amplitudes on the different sites are

$$\overline{a_i^c(t)} = \frac{1}{2^t} \binom{t-1}{\lfloor \frac{t-1}{2} \rfloor}. \quad (\text{C3})$$

Additionally, as a result of the “equalizing” action Eq. (C2), the circuit-to-circuit variance in the conserved amplitudes is suppressed both in the large q and the late t limit:

$$\Delta_i^q(t) \equiv \overline{|a_1^c(t)|^2} - \overline{a_1^c(t)}^2 \sim \frac{1}{q^4} \frac{1}{t^2}. \quad (\text{C4})$$

This can be understood from Eq. (C1) since the difference $\Delta_i^q(t)$ is proportional to the weight of nonconserved terms $\sim |(a_1^c(t) - a_2^c(t))|^2 \sim (\partial_x a_x^c)^2$, which scales as $\sim 1/t^2$ in the region $x \sim \sqrt{t}$ where $a_i^c(t)$ is appreciable Eq. (17). This suppression reflects the “smoothing” action of the circuit which locally makes the averaged amplitudes of the conserved charges equal and thus reduces $(\partial_x a_x^c)$ in time. Further, the additional $(1/q^4)$ suppression comes from the fact that only transitions of nonconserved operators to $[(z\mathbb{I})_i - (z\mathbb{I})_{i+1}]$ contribute to $\Delta_i^q(t)$, and this transition is only one of order q^4 possibilities. Likewise, we can see how this process introduces correlations in the amplitudes a_i^c and a_{i+1}^c and

$$\overline{|a_1^c(t) a_2^c(t)|} - \overline{|a_1^c(t)|} \overline{|a_2^c(t)|} \sim \frac{1}{q^4} \frac{1}{t^2}. \quad (\text{C5})$$

APPENDIX D: TWO-POINT CORRELATIONS OF SPIN AND RAISING CHARGE

We derive Eq. (41) at $q = \infty$. At infinite q , the intergate and intragate correlations of spin and raising charge Eq. (36) have an identical structure, as can be seen from the transition amplitudes in Appendix A. Then, if we work in the frame of the front, so that all distances below refer to distances away from the front location which is t at infinite q , we can easily derive a recursion relation for the steady-state values of G_{ij} Eq. (38), which takes the form

$$G_{2j,2k} = \frac{1}{3} (G_{2j,2k-2} + G_{2j-2,2k} + G_{2j-2,2k-2}). \quad (\text{D1})$$

Because of the even-odd structure of the circuit, the correlations involving odd sites or pairs of even and odd sites can all be derived from the correlations of the even sites alone. Solving this recursion relation by standard methods gives the solution

$$G_{2j,2k} = \frac{1}{3} \sum_{n=k}^{j+k} \left(\frac{1}{3}\right)^n \binom{n}{2n-(j+k)} \binom{2n-(j+k)}{n-j}, \quad (\text{D2})$$

which, after taking care of even-odd effects, reduces to Eq. (41) at $j = k$.

-
- [1] J. M. Deutsch, *Quantum Statistical Mechanics in a Closed System*, *Phys. Rev. A* **43**, 2046 (1991).
- [2] M. Srednicki, *Chaos and Quantum Thermalization*, *Phys. Rev. E* **50**, 888 (1994).
- [3] M. Rigol, V. Dunjko, and M. Olshanii, *Thermalization and Its Mechanism for Generic Isolated Quantum Systems*, *Nature (London)* **452**, 854 (2008).
- [4] P. W. Anderson, *Absence of Diffusion in Certain Random Lattices*, *Phys. Rev.* **109**, 1492 (1958).
- [5] D. M. Basko, I. L. Aleiner, and B. L. Altshuler, *Metal-Insulator Transition in a Weakly Interacting Many-Electron System with Localized Single-Particle States*, *Ann. Phys. (Amsterdam)* **321**, 1126 (2006).
- [6] A. Pal and D. A. Huse, *Many-Body Localization Phase Transition*, *Phys. Rev. B* **82**, 174411 (2010).
- [7] V. Oganesyan and D. A. Huse, *Localization of Interacting Fermions at High Temperature*, *Phys. Rev. B* **75**, 155111 (2007).
- [8] M. Žnidarič, T. Prosen, and P. Prelovšek, *Many-Body Localization in the Heisenberg XXZ Magnet in a Random Field*, *Phys. Rev. B* **77**, 064426 (2008).
- [9] J. Z. Imbrie, *On Many-Body Localization for Quantum Spin Chains*, *J. Stat. Phys.* **163**, 998 (2016).
- [10] D. A. Huse, R. Nandkishore, V. Oganesyan, A. Pal, and S. L. Sondhi, *Localization-Protected Quantum Order*, *Phys. Rev. B* **88**, 014206 (2013).
- [11] D. Pekker, G. Refael, E. Altman, E. Demler, and V. Oganesyan, *Hilbert-Glass Transition: New Universality of Temperature-Tuned Many-Body Dynamical Quantum Criticality*, *Phys. Rev. X* **4**, 011052 (2014).
- [12] J. A. Kjäll, J. H. Bardarson, and F. Pollmann, *Many-Body Localization in a Disordered Quantum Ising Chain*, *Phys. Rev. Lett.* **113**, 107204 (2014).
- [13] R. Vosk, D. A. Huse, and E. Altman, *Theory of the Many-Body Localization Transition in One-Dimensional Systems*, *Phys. Rev. X* **5**, 031032 (2015).
- [14] A. C. Potter, R. Vasseur, and S. A. Parameswaran, *Universal Properties of Many-Body Delocalization Transitions*, *Phys. Rev. X* **5**, 031033 (2015).
- [15] W. De Roeck and F. Huveneers, *Stability and Instability towards Delocalization in Many-Body Localization Systems*, *Phys. Rev. B* **95**, 155129 (2017).
- [16] X. Yu, D. J. Luitz, and B. K. Clark, *Bimodal Entanglement Entropy Distribution in the Many-Body Localization Transition*, *Phys. Rev. B* **94**, 184202 (2016).
- [17] V. Khemani, S. P. Lim, D. N. Sheng, and D. A. Huse, *Critical Properties of the Many-Body Localization Transition*, *Phys. Rev. X* **7**, 021013 (2017).
- [18] V. Khemani, D. N. Sheng, and D. A. Huse, *Two Universality Classes for the Many-Body Localization Transition*, *Phys. Rev. Lett.* **119**, 075702 (2017).
- [19] J. Maldacena, *The Large- N Limit of Superconformal Field Theories and Supergravity*, *Int. J. Theor. Phys.* **38**, 1113 (1999).
- [20] E. Witten, *Anti-de Sitter Space and Holography*, *Adv. Theor. Math. Phys.* **2**, 253 (1998).
- [21] P. Hayden and J. Preskill, *Black Holes as Mirrors: Quantum Information in Random Subsystems*, *J. High Energy Phys.* **09** (2007) 120.
- [22] Y. Sekino and L. Susskind, *Fast Scramblers*, *J. High Energy Phys.* **10** (2008) 065.
- [23] P. Hosur, X.-L. Qi, D. A. Roberts, and B. Yoshida, *Chaos in Quantum Channels*, *J. High Energy Phys.* **02** (2016) 004.
- [24] S. H. Shenker and D. Stanford, *Black Holes and the Butterfly Effect*, *J. High Energy Phys.* **03** (2014) 067.
- [25] N. Lashkari, D. Stanford, M. Hastings, T. Osborne, and P. Hayden, *Towards the Fast Scrambling Conjecture*, *J. High Energy Phys.* **04** (2013) 022.
- [26] D. A. Roberts, D. Stanford, and L. Susskind, *Localized Shocks*, *J. High Energy Phys.* **03** (2015) 051.
- [27] J. S. Cotler, G. Gur-Ari, M. Hanada, J. Polchinski, P. Saad, S. H. Shenker, D. Stanford, A. Streicher, and M. Tezuka, *Black Holes and Random Matrices*, *J. High Energy Phys.* **05** (2017) 118.
- [28] D. A. Roberts and D. Stanford, *Diagnosing Chaos Using Four-Point Functions in Two-Dimensional Conformal Field Theory*, *Phys. Rev. Lett.* **115**, 131603 (2015).
- [29] A. Kitaev, *A Simple Model of Quantum Holography (part 1)*, <http://online.kitp.ucsb.edu/online/entangled15/kitaev/>; *A Simple Model of Quantum Holography (part 2)*, <http://online.kitp.ucsb.edu/online/entangled15/kitaev2/>.
- [30] S. Sachdev and J. Ye, *Gapless Spin-Fluid Ground State in a Random Quantum Heisenberg Magnet*, *Phys. Rev. Lett.* **70**, 3339 (1993).
- [31] A. I. Larkin and Y. N. Ovchinnikov, *Quasiclassical Method in the Theory of Superconductivity*, *Sov. J. Exp. Theor. Phys.* **28**, 1200 (1969).
- [32] E. H. Lieb and D. W. Robinson, *The Finite Group Velocity of Quantum Spin Systems*, *Commun. Math. Phys.* **28**, 251 (1972).
- [33] W. Brown and O. Fawzi, *Scrambling Speed of Random Quantum Circuits*, [arXiv:1210.6644](https://arxiv.org/abs/1210.6644).
- [34] B. Dóra and R. Moessner, *Out-of-Time-Ordered Density Correlators in Luttinger Liquids*, *Phys. Rev. Lett.* **119**, 026802 (2017).
- [35] I. Kukuljan, S. Grozdanov, and T. Prosen, *Weak Quantum Chaos*, *Phys. Rev. B* **96**, 060301 (2017).
- [36] A. Nahum, J. Ruhman, S. Vijay, and J. Haah, *Quantum Entanglement Growth under Random Unitary Dynamics*, *Phys. Rev. X* **7**, 031016 (2017).
- [37] A. Nahum, S. Vijay, and J. Haah, *Operator Spreading in Random Unitary Circuits*, *Phys. Rev. X* **8**, 021014 (2018).
- [38] C. W. von Keyserlingk, T. Rakovszky, F. Pollmann, and S. Sondhi, *Operator Hydrodynamics, OTOCs, and Entanglement Growth in Systems without Conservation Laws*, *Phys. Rev. X* **8**, 021013 (2018).
- [39] Differences between $O_0(t)$ and a random operator are apparent when considering the spectrum of $O_0(t)$, which is highly degenerate and always the same as the spectrum of O_0 due to the unitary time evolution. Also, the operator

- entanglement, although a “volume law,” is only a fraction of that of a random operator [40].
- [40] C. Jonay, D. A. Huse, and A. Nahum, *Coarse-Grained Dynamics of Operator and State Entanglement*, [arXiv:1803.00089](#).
- [41] X. Chen, T. Zhou, D. A. Huse, and E. Fradkin, *Out-of-Time-Order Correlations in Many-Body Localized and Thermal Phases*, *Ann. Phys. (Berlin)* **529**, 1600332 (2017).
- [42] J. Maldacena, S. H. Shenker, and D. Stanford, *A Bound on Chaos*, *J. High Energy Phys.* **08** (2016) 106.
- [43] H. Kim and D. A. Huse, *Ballistic Spreading of Entanglement in a Diffusive Nonintegrable System*, *Phys. Rev. Lett.* **111**, 127205 (2013).
- [44] A. Bohrdt, C. B. Mendl, M. Endres, and M. Knap, *Scrambling and Thermalization in a Diffusive Quantum Many-Body System*, *New J. Phys.* **19**, 063001 (2017).
- [45] D. J. Luitz and Y. B. Lev, *Information Propagation in Isolated Quantum Systems*, *Phys. Rev. B* **96**, 020406 (2017).
- [46] B. Swingle and D. Chowdhury, *Slow Scrambling in Disordered Quantum Systems*, *Phys. Rev. B* **95**, 060201 (2017).
- [47] A. A. Patel, D. Chowdhury, S. Sachdev, and B. Swingle, *Quantum Butterfly Effect in Weakly Interacting Diffusive Metals*, *Phys. Rev. X* **7**, 031047 (2017).
- [48] I. L. Aleiner, L. Faoro, and L. B. Ioffe, *Microscopic Model of Quantum Butterfly Effect: Out-of-Time-Order Correlators and Traveling Combustion Waves*, *Ann. Phys. (Amsterdam)* **375**, 378 (2016).
- [49] J. H. Bardarson, F. Pollmann, and J. E. Moore, *Unbounded Growth of Entanglement in Models of Many-Body Localization*, *Phys. Rev. Lett.* **109**, 017202 (2012).
- [50] V. Khemani, D. A. Huse, and A. Nahum, *Velocity-Dependent Lyapunov Exponents in Many-Body Quantum, Semi-Classical, and Classical Chaos*, [arXiv:1803.05902](#).
- [51] S. Xu and B. Swingle, *Accessing Scrambling Using Matrix Product Operators*, [arXiv:1802.00801](#).
- [52] Note, if the initial operator is Hermitian, the amplitudes $a_i^c(t)$ all remain real, but here we are using absolute value brackets so that the formulas apply even to non-Hermitian operators. Later we will be considering raising and lowering operators which are indeed non-Hermitian.
- [53] C. Rödenbeck, J. Kärger, and K. Hahn, *Calculating Exact Propagators in Single-File Systems via the Reflection Principle*, *Phys. Rev. E* **57**, 4382 (1998).
- [54] T. Rakovszky, F. Pollmann, and C. W. von Keyserlingk, following article, *Diffusive Hydrodynamics of Out-of-Time-Ordered Correlators with Charge Conservation*, *Phys. Rev. X* **8**, 031058 (2018).
- [55] We choose irrational numbers J_x, J_z that are order 1, since this choice has been shown to thermalize better for small system sizes compared to choosing rational parameters [43].